

Microfluidic single cell sorting and trapping using dual spiral channels

by

Pooja Ramesh

A thesis submitted to the graduate faculty
in partial fulfillment of the requirements for the degree of

MASTER OF SCIENCE

Major: Electrical Engineering

Program of Study Committee:
Liang Dong, Major Professor
Nathan Neihart
Jaeyoun Kim

Iowa State University

Ames, Iowa

2010

Copyright © Pooja Ramesh, 2010. All rights reserved.

I dedicate this thesis to my mother, Thriveni Ramesh. Her vision and enthusiasm have taught me to dream and her unfailing support has helped me achieve them.

TABLE OF CONTENTS

LIST OF FIGURES	v
LIST OF TABLES	vii
ABSTRACT	viii
CHAPTER 1. INTRODUCTION	1
1.1 Background	1
1.2 Research motivation	5
1.3 Literature review	6
1.3.1 Particle sorting	6
1.3.1.1 Centrifugation in membranes-less spiral channels	7
1.3.2 Particle trapping	9
1.3.2.1 Centrifugal single cell trapping	9
CHAPTER 2. METHODOLOGY	11
2.1 Proposed cell trapping and sorting using dual-spiral channels	11
2.2 Theory	12
2.3 Device design	17
2.3.1 Stage 1: Curvilinear channels with pockets	17
2.3.2 Stage 2: Spiral channel with pockets	18
2.3.3 Stage 3: Dual spiral channel with pockets	19
2.3.4 Stage 4: Increasing the number of traps in dual spirals	21
2.3 Device modeling and simulations	22
CHAPTER 3. EXPERIMENTS	27
3.1 Fabrication and setup	27
3.2 Experiments with micro-beads	28
3.3 Experiments with animal cells	30
CHAPTER 4. RESULTS AND DISCUSSIONS	33
4.1 Experiments with micro-beads	35
4.1.1 Stage 1: Curvilinear channels with pockets	35
4.1.2 Stage 2: Spiral channel with pockets	36
4.1.3 Stage 3: Dual spiral channel with pockets	37
4.1.4 Stage 4: Increasing the number of traps in dual spirals	39
4.2 Experiments with animal cells	44
CHAPTER 5. CONCLUSION AND FUTURE WORK	47
BIBLIOGRAPHY	50

ACKNOWLEDGEMENTS

LIST OF FIGURES

Figure 1: Schematic and pictures of the spiral microparticle separator. The design has two inlets and two outlets with sample being introduced through inner inlet (7).	7
Figure 2: A) Membrane-free microfiltration with a double spiral design. B) Transition point from one spiral to another (19).	8
Figure 3: Chip design consisting of chamber, channel, valve, and trap (20)	9
Figure 4: Experimental setup from left to right: control module, Charge couple device camera and motor parts for rotating chip (20)	10
Figure 5: Device design with a detailed view of particles travelling in the channel. Particle 1 has a higher probability of getting trapped than particle 2.	11
Figure 6: 3D depiction of a trapped particle in a pocket	12
Figure 7: Secondary flow in a curvilinear channel made up of two counter-rotating vortices perpendicular to the primary flow direction	13
Figure 8: Illustration of the Dean vortices and the differential particle migration in cross sectional view (7).	15
Figure 9: Curvilinear channels to test particle migration lined with pockets on the outer wall. (Images not drawn to scale)	18
Figure 10: Design of spiral microfluidic channel with pockets lining the outer wall	19
Figure 11: Dual spiral channel (secondary/reservoir channel)	20
Figure 12: Depicts the dual spiral device with a very high density of traps. Figure on the left has higher density of traps in each spiral than the one on the right.	22
Figure 13: Static Pressure in the channel	24
Figure 14: Velocity vectors depicting the fluid flow in the channel	25
Figure 15: Tracing of the trajectory of a particle. It predicts where the particle will get trapped.	26
Figure 16: 3D view of the spiral device	28
Figure 17: A) Depicts a trapped and immobilized particle B) Picture of a trapped and immobilized 30 μm glass bead.	29
Figure 18: Picture showing cells that have migrated to the outer wall at Spiral 2 at a flow rate of 2.0mL/hr.	31
Figure 19: Picture of the cell migrating towards the pocket.	31
Figure 20: Picture of a cell trapped at the opening of the pocket	32
Figure 21: Curvilinear channel with pockets. No trapping obtained.	36
Figure 22: Demonstrates the migration of particles from inner wall towards the outer wall as they move from the first spiral (close to inlet) to the fifth spiral (close to outlet). These images belong to frames of a video recorded when a mixture of water and 15 μm polystyrene beads was continuously injected into the channel at a speed of 1.2 mL/hr.	37
Figure 23: Still image from a video depicting polystyrene beads flowing past a filled pocket without entering the pocket. This demonstrates single trapping.	39
Figure 24: Collage containing picture snapshots taken radially outward for the 2 nd spiral to the 5 th spiral showing trapping in each spiral.	40

Figure 25: Collage containing picture snapshots taken radially outward for the 2 nd spiral to the 5 th spiral showing trapping in each spiral (different location in the spiral)	41
Figure 26: Crowding or accumulation of beads at pockets located in the first and second spiral noticed only when the flow rate is high (above 2.0 mL/hr)	44
Figure 27: Single cell trapping using adult rat hippocampal stem cells when injected at the rate of 2.0 mL/hr. The concentration of the mixture used was 10 ⁵ cells/mL.	45

LIST OF TABLES

Table 1: Dean Drag force experienced by particles at each radius of curvature for different injection rates of 15 μ m polystyrene particles.	34
Table 2: Inertial Lift force experienced by particles at different fluid velocities	35
Table 3: Trapping Efficiency of pockets at each spiral	42
Table 4: Trapping site occupancy based on flow rate.....	46
Table 5: Summary of single cells analysis, properties of interest and method of analysis	49

ABSTRACT

The recent research and development of microfluidic systems for biological and chemical analysis has enabled interfacing and analyzing single or small population of biological cells. In this thesis, we describe a passive microfluidic device with dual spiral geometry for the separation and single cell trapping from a heterogeneous mixture. The device makes use of two spirals to sort and trap cells. Cells flowing in the primary channel experience centrifugal acceleration as they travel along the spiral. A combination of Dean drag force and inertial lift force acting on the cells in the primary channel, cause them to migrate towards the outer wall. The outer wall is lined with traps to capture single cells that have laterally migrated due to centrifugal force. A local suction force is created at each trap by the use of the secondary spiral channel to provide an additional lateral force to assist in cell trapping. The microfabricated devices were tested with polystyrene microbeads, glass microbeads and adult rat hippocampal stem cells at various microfluidic conditions. Using the proposed technology, an average trapping efficiency of >50% was achieved. Besides providing a high trapping efficiency, this unique dual-spiral configuration has the potential to facilitate single-cell studies by providing a convenient way to load /unload agent and reagent solutions through the secondary channel and to create a concentration gradient of factors in both the primary and secondary channels.

CHAPTER 1. INTRODUCTION

1.1 Background

There has been a lot of interest in recent years in studying and quantifying a wide range of biological responses of individual cells rather than bulk. Within multicellular organisms, each individual cell continuously receives both endogenous (originating within) and exogenous (originating from outside) signals that regulate their behavior. Although *in vitro* culture systems have been present for many decades now, it is significantly different from *in vivo* conditions. *In vivo*, the cells reside in a tissue microenvironment and interact with various microenvironment factors such as the extra cellular matrix, other cells, and various soluble factors which are different from *in vitro*, where the cells are exposed to bulk culture environments. Hence, the development of systems or methods which provide better interactions between the micro-environment and cells are needed. These systems or methods will incorporate cells into components of a controlled micro-environment to mimic their natural micro-environment and thus, improving our understanding of cell behavior *in vivo*.

Single cell techniques have revealed key elements of otherwise invisible processes like chemical transfer, new insights of chemical signaling pathways and mechanisms behind the coordination of multicellular behaviors. They have enabled the study of discrete and dynamic events within living cells like the diffusion process in autocrine and paracrine signaling and the effects of secreted soluble factors in the cell microenvironment (1). Direct measurements at micro and nano-scales of the mechanical properties of individual cells like turgor pressure, elasticity and bursting force have also been achieved (2), (3).

The recent study and development of microfluidic systems has enabled interfacing and analyzing single or small population of cells. Microfluidics is the science and technology of systems that process or manipulate small (10^{-9} to 10^{-18} litres) amounts of fluids, using channels with dimensions of tens to hundreds of micrometers (4). Microfluidics has been applied in many disciplines so far (e.g. chemistry, medicine, biology) and has shown the following significant advantages:

- cost savings owing to low reagent and sample volumes and to low-cost disposable devices;
- highly sequential or parallel experimentation;
- better mimicry of the natural tissue environment and precise experimental control of the cellular microenvironment (5).

Microfluidics has already proven to be successful in genetic and proteomic analysis and can be extended to cell analysis. These microdevices with low system complexity provide the ability to interface cells which makes biological and chemical analyses possible. Apart from reduced system complexity, the miniaturization in microfluidic devices has numerous benefits; including, reduced cell consumption, automated and reproducible reagent delivery which are crucial while testing new and expensive drugs and thereby improve the performance.

Another process that often happens prior to cell analysis in microfluidic devices is cell sorting, separation or removal of target cells from the original mixture. Separation and filtration have many applications in biological and environmental assays, micro/nano-manufacturing, and clinical analysis. Separation and filtration of microparticles is performed based on size (6), (7), physical properties (8) and internal fluidic shear characteristics. In

order to isolate and analyze single cells, the commonly used methods of manipulation can be categorized based on the manipulating force employed i.e., mechanical, electrical, optical, magnetic.

The main principle of on-chip mechanical manipulation is the separation of target cells using microfluidic structures. Separation of cells within the microchannels can be achieved by fabricating constriction structures such as microfilters (9), microwells (10), microgripper (11), or by modifying microchannel interior surface with reactive coating, with antibodies, with selectin and with enzymes. Mechanical trapping of cells has been achieved by microfabricated mechanical filters which trap different cell types from whole blood. The filters were made of arrays of rectangular parallel channels which would not allow particles larger than the channel to enter. But this is an inefficient method for separating a wide range of particles since the pore size is a fixed dimension. Carlson et al. (8) and Bakajin et al. (12) have used hydrodynamic forces to move the blood through a lattice of filters embedded in the channels. The difference in physical properties between white blood cells – extremely sticky and red blood cells – non-adhesive facilitates easier trapping and separation of the two kinds of primary cells present in blood. While the red blood cells readily penetrate and pass through the lattice, the white cells are greatly retarded and eventually adhere to the surface. Though such physical property differences can be beneficial, they can also pose as a major challenge while trying to achieve separation. For example, the hydrophobic surface of the channel wall allows hydrophilic protein ends to adhere to it. Another mechanical approach is the use of micropipettes by Rusu et al. who direct beads towards optical traps from which they are then drawn out (13). Another technique used by Khademhosseini et al. (10) was to fabricate microwells within microchannels which are used to collect cells within pre-defined

locations. Chronis and Lee (11) have developed a microfluidic device with a SU-8 based microgripper that could manipulate single cells in physiological ionic solutions and hold a cell without exerting any forces in the closed position.

Electrical trapping consists of the electric-field to separate cells where in, depending on the nature of the bioparticles to be manipulated, either a dc field for electrophoresis of charged particles, or a non-uniform ac field for dielectrophoresis of polarizable particles is used. The standard way to make a dielectrophoresis trap is to create an electric field gradient with an arrangement of planar electrodes either connected to a voltage source or free-floating in the presence of an ac field. This technique is the best suited for miniaturization because of the relative ease of microscale generation and structuring of an electric field on microchips. Electrophoresis or dielectrophoresis have been employed to attract, confine and hold cells from the fluid flow in microchannels consisting of micro/nanopores or single cell traps. This enables localization of a single cell on top of the pore or in a trap where they can be analyzed. Arai and co-workers (14) developed a system for separation of a single micro-organism from a large number of microbes in a microfluidic device using both a laser trapping force and a dielectrophoretic force.

Optical manipulation of biological species on microfluidic devices has been gaining more interest due to its non-contact and contamination-free manipulation process. Optical tweezers can bind biological molecules to dielectric spheres and then capture the spheres at the focal point of an electric field gradient. Umehara et al. (15) employed optical tweezers to position bacterial cells in a single cell cultivation assay where the single bacterial cells could be isolated and positioned in microchambers. Biological particles are optically trapped using optical tweezers which offer high resolution for single cell trapping. Optical traps are also

created by trapping the target cell at the focal point of the laser trap and by using an electrical field to exclude excess cells (16).

Magnetic manipulation is commonly used method for cell separation in microfluidic devices where magnetic particles are selectively attached to cells. The commonly used super-paramagnetic beads are 10-100nm in diameter, whose extremely small size makes them very gentle on cells with no apparent effect on cellular function and cell viability. Magnetic field gradients generated by various methods are employed to capture the bead and, consequently, the cell attached to the bead, because of the magnetic anisotropy inherent in the paramagnetic beads. The high specificity and efficiency of magnetic methods make them quite useful in obtaining rare cell types, especially in handling red blood cells (17). Westervelt and co-workers (18) embedded a microelectromagnetic matrix into a microfluidic device to develop various methods to manipulate biological cells. The magnetic field generated by the matrix can stably control individual cells in the fluid and be configured dynamically.

1.2 Research motivation

After a broad overview of the current technologies available in sorting and trapping cells, the advantages and disadvantages stand out clearly. Many of these technologies are not entirely lab-on-chips, requiring additional electronics or optics to support the operation of the device. From this perspective, a case can still be made for the need of a microfluidic device that can firstly, sort target cells from the original liquid with no need for a prior preparation of original mixture of any particular kind; secondly, traps individual cells in microchambers; thirdly, is easy to fabricate mainly requiring only soft lithography and lastly, does not require additional electronics or optics with no requirement of a prior device treatment for successful

operation and trapping of cells; lastly, convenient loading/unloading of micro-environmental soluble cues and provision to create a concentration gradient of these cues, benefiting biologists to study cell migration differentiation, and proliferation in a subtly controlled micro-environment.

The microfluidic device that is developed in this thesis satisfies all the above four criteria by using centrifugal force and lift forces generated in spiral channels to sort and trap cells; can be used on a variety of cells of different shapes and sizes due to the use of membrane-less sorting and filtration; is fabricated using a conventional soft lithography microfabrication process; and does not require any additional electronics other than a basic syringe pump to inject fluid into the microfluidic channels.

1.3 Literature review

Below is a literature review of technology over the past 2 years developed for devices that employ centrifugal force to sort particles and devices that trap cells using the same principle.

1.3.1 Particle sorting

Biological cells or micro-meter sized particles have been separated from the original mixture using spiral/curvilinear microfluidic channels. This has been done in two ways: by using membranes to filter out the desired cell/particle size and membrane-less where particles get separated based on the mass and size. Use of membranes to filter out the particle limits the range of particles that can be separated because the pore size of the membrane is a fixed

device dimension. Hence in the following sub-section, we will take a look at separation achieved without the use of membranes.

1.3.1.1 Centrifugation in membranes-less spiral channels

Ian Papautsky and coworkers (7) have achieved separation of two particle sizes $7.32\mu\text{m}$ and $1.9\mu\text{m}$ particles using a 5-loop spiral microchannel (Figure 1). The design takes advantage of the inertial lift and viscous drag forces that act on the particles causing differential migration and hence separation of these microparticles. The inertial forces and rotation force due to the spiral microchannel geometry cause the larger particles to occupy a single equilibrium position near the inner microchannel wall and the smaller particles are transposed to the outer wall. This combined effect of the forces acting on the two particle sizes results in the formation of distinct particle streams based on their size, which is in turn collected at separate outlets by taking advantage of the laminar flow in the microchannel. The spiral microchannel is fabricated using standard soft lithography methods.

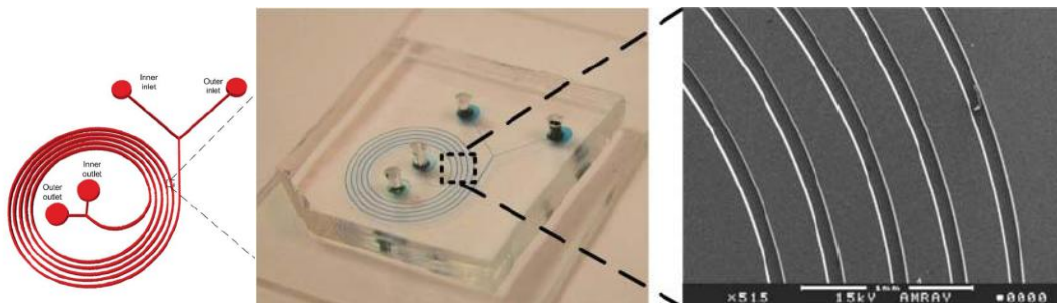


Figure 1: Schematic and pictures of the spiral microparticle separator. The design has two inlets and two outlets with sample being introduced through inner inlet (7).

An alternative design employing the same principal of centrifugation where lateral forces across the spiral channel transform a homogenous distribution of particles at the inlet

area into an ordered band near the outlet is described by (19). The design consists of a double spiral as seen in Figure 2.

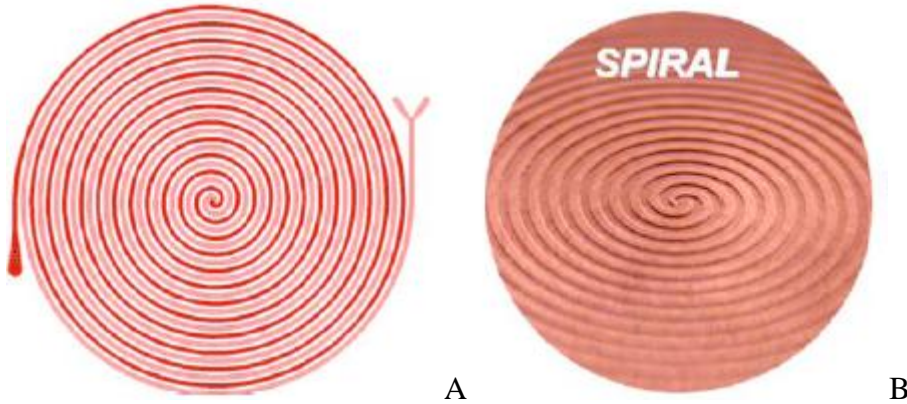


Figure 2: A) Membrane-free microfiltration with a double spiral design. B) Transition point from one spiral to another (19).

A homogenous mixture is passed through the inlet and as it reaches the transition point, a sharp band is formed on the inside due to compacting effects of centrifugal and lift forces and a more diffuse band is formed on the outside. Passing through the transition point which changes the flow direction from clockwise to counterclockwise, the sharp band switches to the outside and diffuse band is switched to the inside. This diffuse inner band is subjected to centrifugal force and becomes a sharp band which continues following through the channel. The diffuse band consisting of particles of the smallest size is collected at the outlet. This process continues as each particle size is separated starting from the smallest. Hence, the advantage of this spiral design is the large dynamic size range that can be filtered.

1.3.2 Particle trapping

1.3.2.1 Centrifugal single cell trapping

Sung-Woo Lee and co-workers (20) have developed a single cell assay within compact disc like lab chip with trapped single cells by centrifugal force. A compact disc like chip was made from PDMS which consisted of microchambers and microchannels lined with pitfalls at the edges as show in the Figure 3.

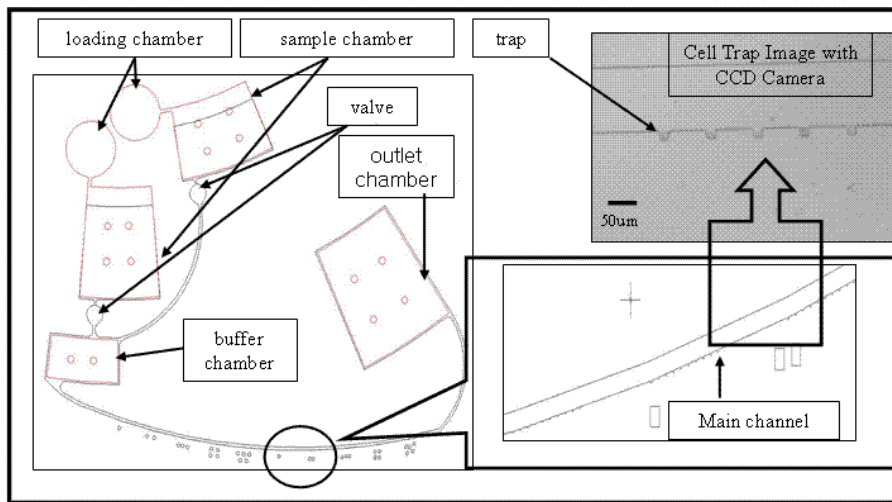


Figure 3: Chip design consisting of chamber, channel, valve, and trap (20)

This CD was loaded on a motor and was rotated at the speed of 1200rpm for 120 seconds. When the CD was rotated, the centrifugal force provided by the rotation pushed the cells outward into the traps. The centrifugal force also allowed keeping the cells in place once they were trapped. A trapping efficiency of 80% was obtained. The setup is shown in Figure 4. As seen below, the operation of this device depends largely on external electronics.

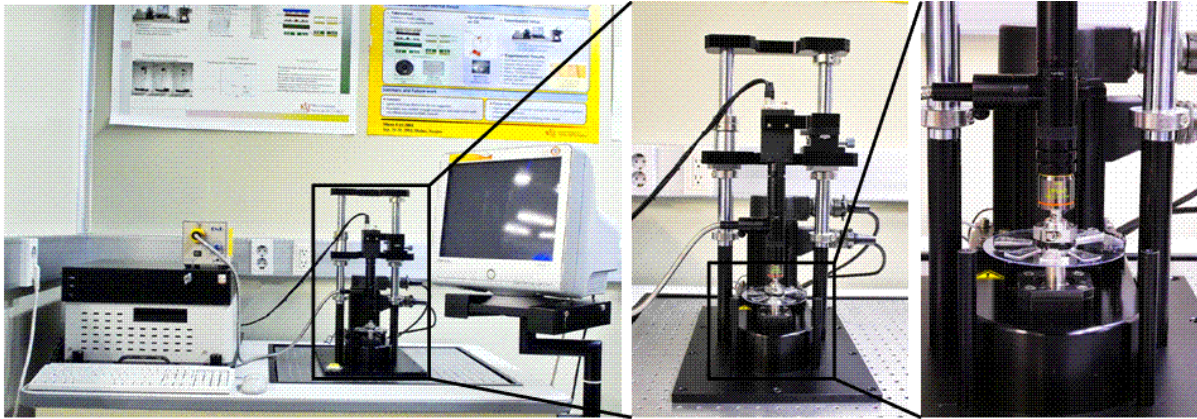


Figure 4: Experimental setup from left to right: control module, Charge couple device camera and motor parts for rotating chip (20)

There are main disadvantages of using centrifugation to trap cells as done by Sung-Woo Lee and co-workers described above requires additional electronics, high rotation speeds of 1200rpm for 2 minutes. Damage done to cells when they collide with the channel walls at such high rotation speeds has not been determined. Though the fabrication is simple, it does not offer a complete lab-on chip platform.

CHAPTER 2. METHODOLOGY

2.1 Proposed cell trapping and sorting using dual-spiral channels

Our proposed design for cell trapping and sorting consists of two concentric spirals – primary channel and a secondary (reservoir) channel. The outer wall of the primary channel is lined with pockets to trap cells. Depending on the location of the particle from the pocket, the probability of getting trapped varies. As seen in Figure 5, particle 1 has a higher chance of getting trapped when compared to particle 2. In other words, particles closer to the pocket experience a greater suction force. The reservoir channel is connected to each pocket and provides the suction force to trap a particle. A vacant pocket does not produce local turbulence in the channel flow and the particles further away from the pocket continue to flow forward in their respective laminar streams as seen Figure 5.

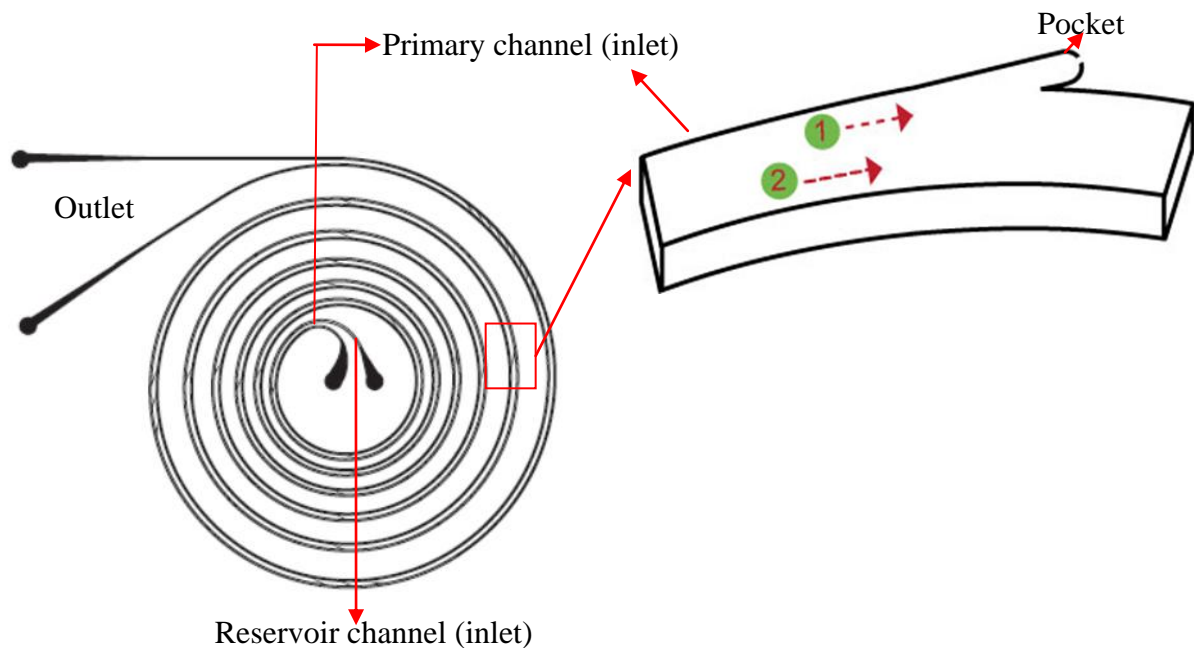


Figure 5: Device design with a detailed view of particles travelling in the channel.

Particle 1 has a higher probability of getting trapped than particle 2.

The way the pockets are designed is to have an opening that leads into the reservoir channel. Owing to this design feature of the pocket, the trapped particle almost entirely blocks the opening, causing considerable decrease in the suction force. This prevents additional particles from getting trapped and ensures single trapping.

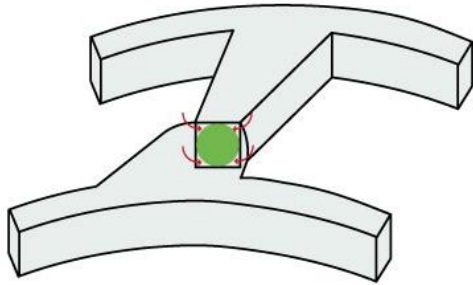


Figure 6: 3D depiction of a trapped particle in a pocket

With this design, trapping can be achieved without the need for a very large centrifugal force generated by an external motor it also offers flexibility to sort target cells from the original mixture and trap these cells. Thereby, it does not limit the size of the particles to be sorted and trapped. The opening of the pocket is kept minimum so that this design can accommodate a variety of cell sizes.

2.2 Theory

In curvilinear channels, there is a mismatch of velocity in the downstream direction between fluid in the center and near-wall regions, which creates a secondary flow. Fluid elements near the channel centerline, have larger inertia than fluid near the channel walls, and hence tend to flow outward around a curve, creating a pressure gradient in the radial direction of the channel. Since the channel is enclosed, relatively stagnant fluid near the walls re-circulates inward due to this centrifugal pressure gradient, creating two symmetric vortices

in the top and bottom halves of the channel (Figure 7) (21). These vortices, caused due to the centrifugal acceleration experienced by the fluid in curvilinear channel, are known as Dean Vortices. The flow is characterized by the Dean Number.

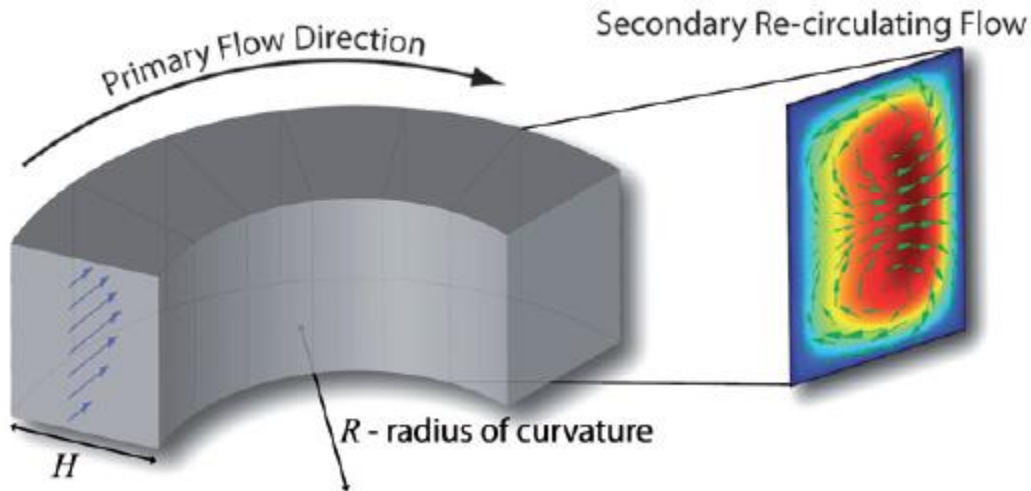


Figure 7: Secondary flow in a curvilinear channel made up of two counter-rotating vortices perpendicular to the primary flow direction

A dimensionless number, Dean Number (De) was first established by W. R. Dean and the generally accepted form of the Dean number by Berger et.al (22). The magnitude of the flow is quantified by the Dean number and is given by:

$$De = \frac{\rho * U_f * D_H}{\mu} \sqrt{\frac{D_H}{2R}} = Re \sqrt{\frac{D_H}{2R}} \quad \text{Equation 1}$$

where, ρ is the density of the fluid medium (Kg/m^3), U_f is the average fluid velocity (m/s), D_H is the diameter/width of the microchannel, R is the radius of curvature and Re is flow Reynolds number. For a straight microchannel, $De = 0$, indicating the absence of Dean flows. In curved channels, De increases with higher curvature (smaller R), larger channel size

(larger D_H), and faster flows (higher Re). Depending on the particle size, this drag force (F_D) causes particles to move along the Deans vortices and consequently more towards the inner or outer channel walls. The drag force can be mathematically expressed as:

$$F_D = f_L * \rho * U_f^2 * \frac{a^4}{D_H^2} = 5.4 * 10^{-4} * \pi \mu D e^{1.63} a_p \text{ (N)} \text{ Equation 2}$$

where, a , is the diameter of the particle and the proportionality constant f_L , a non-dimensional lift co-efficient, is a function of the Reynolds number and the normalized cross-sectional position (23), (24).

In addition to the Dean Drag force F_D , particles in the curvilinear channel experience pressure forces and inertial lift forces (F_L) that are inherent to confined channels (25). The net lift force acting on the particles is a combination of the sheer-induced inertial lift force and wall-induced inertial lift force and it acts perpendicular to the main channel flow. Key parameters which control the magnitude and direction of the lift forces are channel dimensions, channel aspect ratio, particle diameter and flow rate. The inertial lift force F_L acting on the particles also depends on the cross-sectional position of the particle within the microchannel and Re . The lift force can be mathematically expressed as:

$$F_L = \rho G^2 C_L a_p^4 \text{ (N)} \text{ Equation 3}$$

where, G is the shear rate of the fluid (s^{-1}) and C_L is the lift co-efficient which is a function of the particle position across the channel cross-section. The average value of G for a Poiseuille flow is given by $G = U_{max}/D_H$, where, U_{max} is the maximum fluid velocity (ms^{-1}) and can be approximated as $2 * U_f$.

A combination of Dean Flow and inertial lift can provide precise focusing and positioning of particles. Key external parameters to control the particle focusing behavior include the channel dimensions, aspect ratio and radius of curvature, particle diameter and flow rate. As a first order approximation for particles flowing in curved channels, one can assume that the effects of inertial migration and secondary flow act in superposition on the particle (26). Particles dispersed in a spiral microchannel get drawn into one of the two Dean vortices that are formed at the top and bottom half of the microchannel (Figure 8).

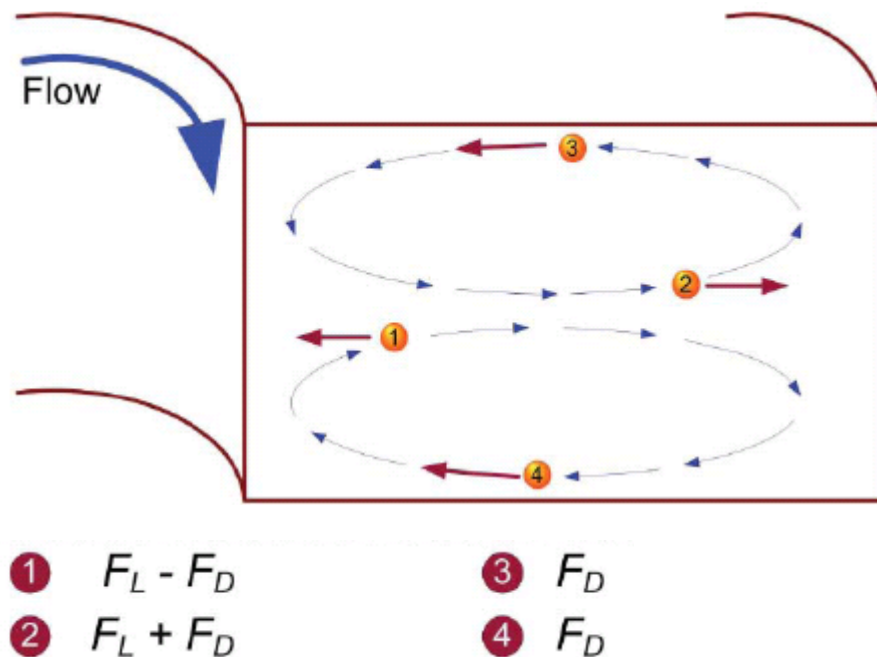


Figure 8: Illustration of the Dean vortices and the differential particle migration in cross sectional view (7).

Particles flowing near the top and bottom of the microchannel at positions 3 and 4 will experience strong lateral flows due to the Dean Drag force and are either pushed towards outer or inner walls of the microchannel. Near the outer wall near position 2, the net lift force acts along the direction of the dean drag force and the particle continues to follow the Dean

vortices independent of their size. If the ratio of a/D_H is < 1 , an assumption can be made that the particle flow does not disturb the secondary flow field. At position 1 where the lift forces and the dean drag force are in opposing directions, depending on the magnitude of these forces, the particles will either equilibrate and form a focused stream or continue to recirculate in the Dean's vortex.

In short, the ratio of the inertial lift and Dean drag is a key parameter to predict the behavior of such systems. An inertial force ratio:

$$R_f = \alpha^2 * \frac{R}{D_H^3} \quad \text{Equation 4}$$

This equation describes the order of magnitude scaling between these forces by dividing the dimensional scaling of inertial lift in the shear gradient region (27) with the scaling of Dean Drag, neglecting any position and Re-dependent changes (28). This dimensionless number is useful in predicting particle behavior:

- a. $R_f = 0$ – particle streams will remain in secondary flow by without attaining inertial equilibrium positions
- b. $R_f = \infty$ - in cases where the particle Reynolds number is high, particles will migrate to inertial equilibrium positions independent of secondary flows

When R_f is intermediate, inertial equilibrium positions can be modified by the secondary flows giving rise to new focusing modes. Also since R_f is dependent on size, two different sized particles in the channel can experience different behaviors in a channel with the smaller particles getting carried into the secondary flow while larger particles is focused at inertial equilibrium positions.

With this knowledge, key parameters like channel dimension, radius of curvature and the diameter of the particle of interest can be used to design a spiral channel where the position of the particle focus band across the width of the channel can be determined. This fundamental idea of achieving a focused band of same sized particles is indeed the phenomenon of separation of particles from the original medium and using the flexible system design of microfluidic applications, these focused bands can be routed to different areas of a lab-on-chip for further processing.

2.3 Device design

Below is the design process in stages from the time the concept was conceived till the development of a successful sorting and trapping device.

2.3.1 Stage 1: Curvilinear channels with pockets

With the theoretical knowledge that particles travelling in a curvilinear channel undergo lateral migration and form a focused band, a variety of curvilinear channels were designed (Figure 9) with the intention to cause particles will migrate towards the outer wall of the channel. The outer wall of the channel was designed to be lined with pockets/traps which would collect single cells travelling close to the outer wall. The width of the pockets was designed to be approximately 1.5 times the diameter of the particle/cell. Each of the designs below have different radius of curvature and channel length.

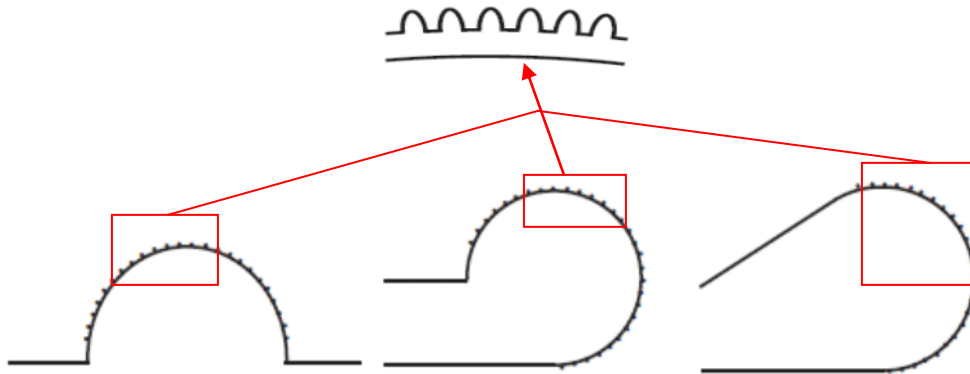


Figure 9: Curvilinear channels to test particle migration lined with pockets on the outer wall. (Images not drawn to scale)

2.3.2 Stage 2: Spiral channel with pockets

In order to provide sufficient channel length for lateral migration, the curvilinear channels were extended to spiral channels (Figure 10). Increasing the channel length and having an decreasing radius of curvature, causes particles to migrate faster and occupy equilibrium positions in shorter channel distances. 4, 5, 6 spiral channels were designed and as before the outer wall of the spirals were lined with pockets. The width of the pockets was designed to be approximately 1.5 times the diameter of the particle/cell.

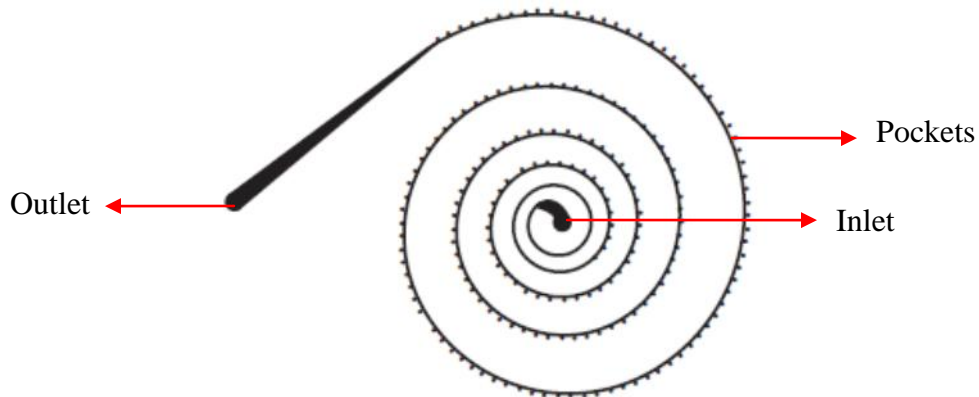


Figure 10: Design of spiral microfluidic channel with pockets lining the outer wall

2.3.3 Stage 3: Dual spiral channel with pockets

Buoyant particles migrate towards the outer wall and form a focused stream. Laminar flow in the channel allows these particles to continue following in their streams along the spirals seen in Stage 2. As they enter the pocket the stream contours along the walls of the pockets and continues on with the main channel stream without any chaotic flow at low Reynolds number. Hence the particle, unless otherwise, follows the fluid drag and flows into the pocket and subsequently out of the pocket. In order to hold the particle in place within the pocket and/or cause it to enter the pocket, a local suction force has to be created that sucks an approaching particle into the pocket and fixates that particle inside the pocket.

In order to provide a pressure difference and add a suction force, a secondary/reservoir channel was added to the 5- spiral design, illustrated in **Figure 11**. The width of the primary and reservoir channels is $180\mu\text{m}$. This reservoir channel runs parallel to the main channel. Each pocket is connected to the reservoir channel. The size of the pocket is approximately $30\mu\text{m}$. It opens up into a tertiary channel and this tertiary channel terminates

at the reservoir channel. The opening at the pocket is smaller than the diameter of the target particle causing the particle to get trapped in the pocket and not enter the reservoir channel. The reservoir channel also consists of an inlet and outlet. By keeping the inlet closed and exposing the outlet to atmospheric pressure, a pressure difference between the two main channels (primary and reservoir) is created, where, the primary channel has fluid being pumped into it, causing high pressure, and the reservoir channel has comparatively a low pressure due to the closed inlet. This pressure difference that exists between the two channels causes the fluid from the main channel (locally) to rush into each pocket to the reservoir channel to equalize the pressure. Particles present near the pockets also get dragged into the pocket during this process. Due to the fact that the opening in the pocket is much smaller than the particle, the particles get trapped. Pockets have been designed to be at a 45° angle with the channel in the direction of fluid flow making it easier for particles to enter the pocket as seen in Figure 11.

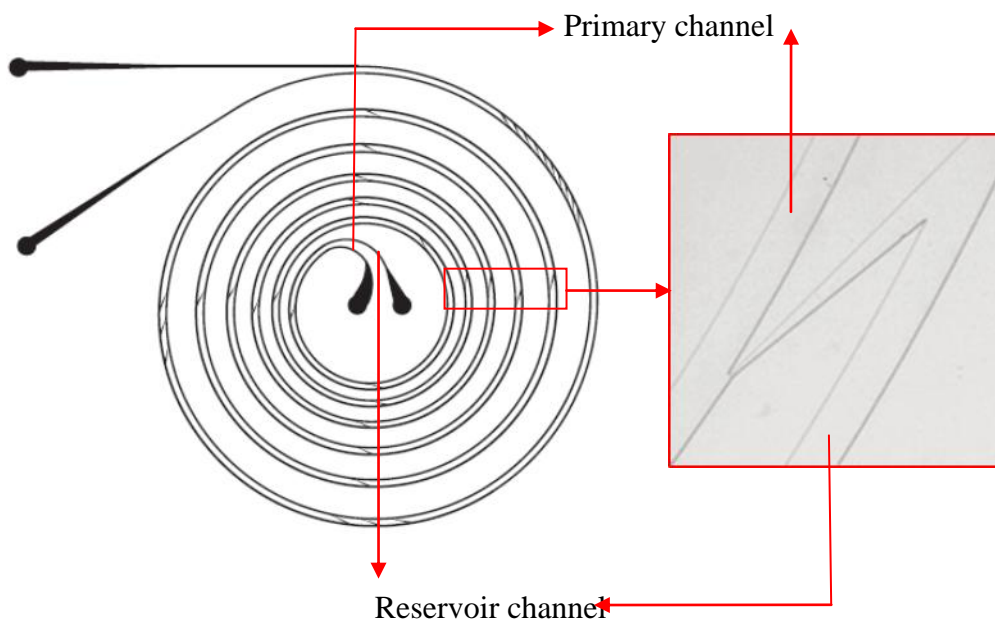


Figure 11: Dual spiral channel (secondary/reservoir channel)

At stage 3, a complete design was achieved. The working of this device design is based on the lateral migration of the particles caused by the centrifugal acceleration and lift forces and the trapping of particles aided by the local suction created at each pocket. In detail, particles flowing through the spiral experience a large centrifugal force (which decreases as they move towards the outlet) due to the small radii of curvature. This causes particles to move closer towards the outer wall. A pressure gradient is developed beginning at the opening in each pocket and terminating at the secondary channel. The fluid near each pocket rushes into the pocket to balance the pressure difference between the primary channel (high pressure) and reservoir channel (low pressure). As a particle approaches a pocket, it gets carried by this fluid flux moving radially outward into the pocket. The particle cannot enter the opening in the pocket since the size of the particle is higher than the size of the opening. Hence, the particle gets trapped in the pocket and is not allowed to enter the reservoir channel. The proof of this theory will be provided by software simulations and experimental observations and data.

2.3.4 Stage 4: Increasing the number of traps in dual spirals

In the previous design, a pocket existed at every curvature change and single trapping could be achieved on every spiral. In order to increase the trapping efficiency, the designed was optimized by increasing the density of traps on each spiral as seen in Figure 12. The first loop in the spiral consists of over 30 traps, the second and third loops in the spiral consists of over 40 traps and the fourth and fifth loops in the spiral consists of greater than 60 traps. Each device in Stage 4, on an average consists of over 250 traps.

Also, it is interesting to find out that a dense distribution of traps does not invalidate the proposed mechanism and does not affect trapping. Addition of traps does not affect fluid flow in the channel. Particles continue to experience a lateral migration as they shift outward and a local sucking force is still generated at each pocket across the tertiary channel of connecting duct. Proof of these statements is provided in the CHAPTER 4.

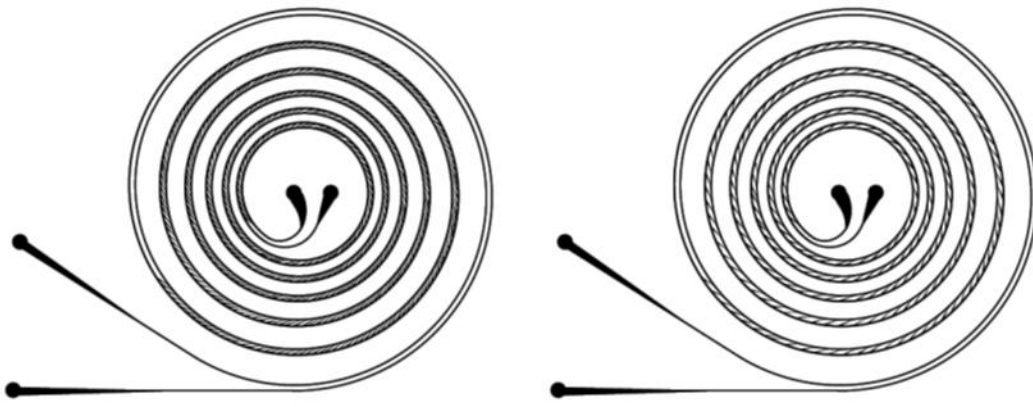


Figure 12: Depicts the dual spiral device with a very high density of traps. Figure on the left has higher density of traps in each spiral than the one on the right.

2.3 Device modeling and simulations

Theoretical modeling of the spiral device (Figure 11) was performed using the computation fluid analysis software Ansys Fluent. The simulation environment was set up for incompressible, laminar flows. The physical properties of water were (density $\rho = 1000 \text{ kg m}^{-3}$ and dynamic viscosity $\mu = 10^{-3} \text{ kgm}^{-1}\text{s}^{-1}$) applied to the simulation. Polystyrene particles $15\mu\text{m}$ in diameter were dispersed into the flow stream at the inlet. By assigning a

zero input velocity, the particles were forced to flow at the same velocity as the fluid at the inlet.

Starting with an AUTOCAD drawing of the device with a pocket at each spiral, ICEM was used to create meshes. Each surface of the device was named. This was imported into Fluent, and boundary conditions were set on each surface. The walls were made incompressible. The inlet of the primary channel was set to a mass flow rate of $2e-7$ Kg/s (~ 0.7 mL/hr) and the outlet was set to atmospheric pressure. The inlet pressure of the secondary channel was set to stationary wall with no slip conditions and the outlet was set to atmospheric pressure. Discrete phase analysis was performed using an injection mode to inject water and particles. Calculations were performed to plot the velocity vector, pressure and particle tracing.

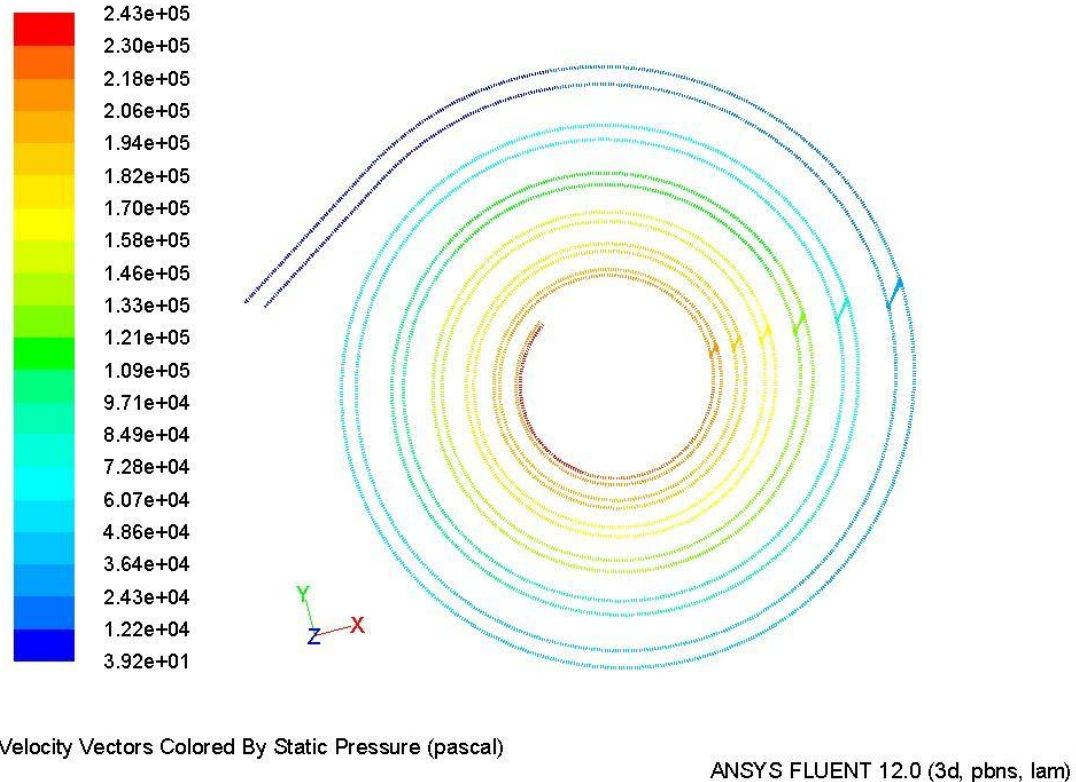


Figure 13: Static Pressure in the channel

The pressure in the channel is maximal at the inlet of the primary channel where the fluid is injected, and it is minimal at the outlets. As seen in Figure 13, there exists a pressure difference between the primary and secondary channels at each pocket. This difference gradually decreases as the spiral number increases. The maximum difference is noticed at the first spiral (closest to the inlet). Lower the pressure difference between the primary and secondary channels, lower is the trapping probability. This is depicted by the velocity vector plot shown in Figure 14. The density of the lines is higher in the pocket on the left (belonging to the 1st spiral) when compared to the pocket on the right (belonging to the 2nd spiral). The flux near each pocket is responsible for pushing the particle into the pocket. Stronger the flux near the pocket, easier is the trapping.

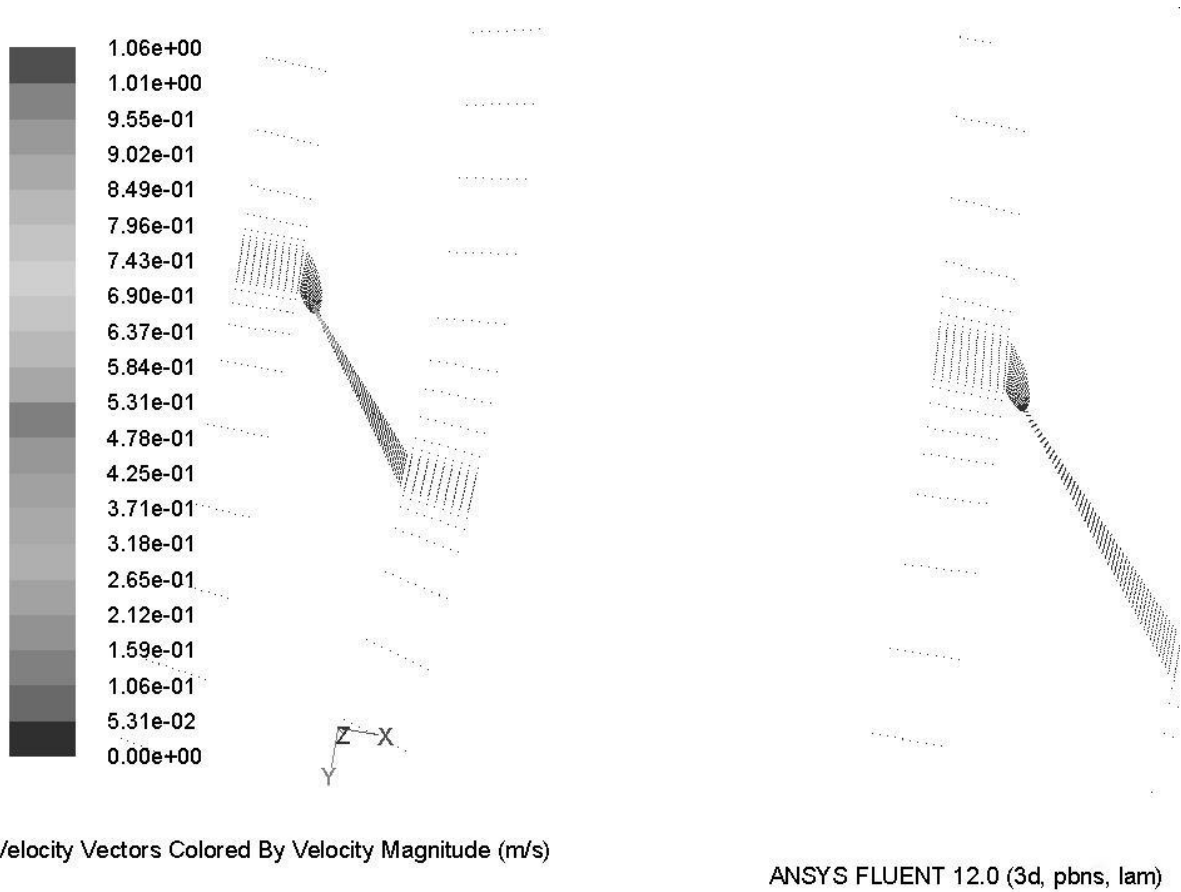
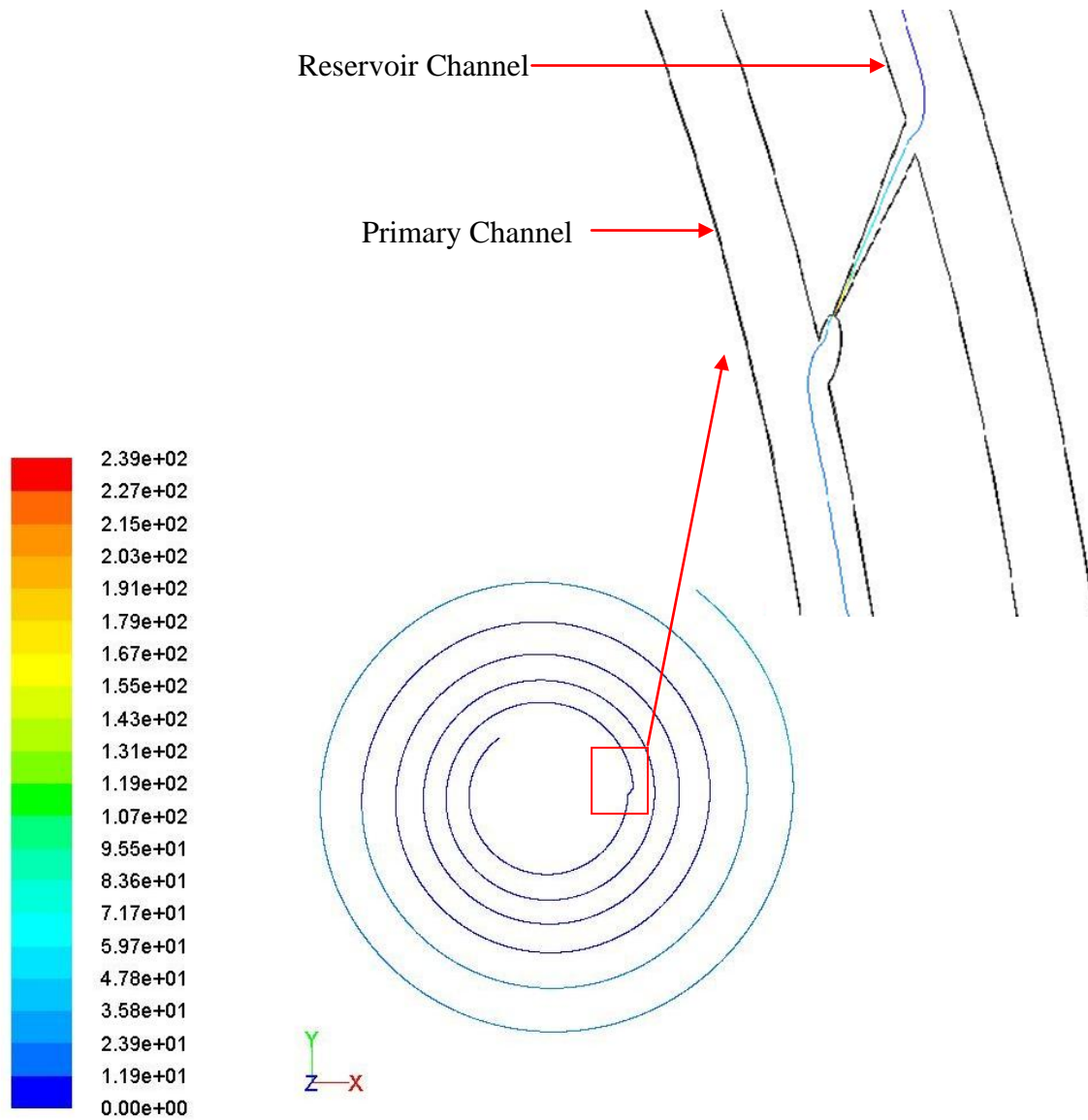


Figure 14: Velocity vectors depicting the fluid flow in the channel

The software also provides an option to trace the particle as it moves along the channel. As seen in Figure 15, the particle gets trapped at the pocket in the first spiral. The velocities projected by the software are higher than velocity of the particle calculated using the equations in 2.2 Theory. This is because the model does not account for both the inertial lift and the Dean drag to contribute to the particle trapping.



Particle Traces Colored by Particle Residence Time (s)

ANSYS FLUENT 12.0 (3d, pbns, lam)

Figure 15: Tracing of the trajectory of a particle. It predicts where the particle will get trapped.

CHAPTER 3. EXPERIMENTS

3.1 Fabrication and setup

The 5- spiral microchannel was fabricated using standard soft lithography (29). 25 μ m thick SU-8 (25, Micro Chem Co) was spin coated on a clean single side polished 3” silicon wafer and patterned using conventional photolithography. A mixture of 10:1 of PDMS and curing agent (Sylguard 184 Elastomeric kit, Dow Corning) was degassed and poured over the SU-8 mold. After the PDMS hardened, it was peeled off to obtain a replicated device structure. Using a 14 gauge metal needle, ports were punched at the inlet and outlet of the channels. The exposed microfluidic channel was sealed by bonding the PDMS structure to a microscope glass slide (75x50mm, Fisher Scientific) by placing the two in air plasma for 50seconds. This created permanent bond between the glass and the PDMS. The device was then placed in a conventional oven at 50°C for 20 minutes to harden the bond between glass and PDMS. Connectors were made using PDMS (30) to provide a flexible connection between the tubing used to inject fluids and the device ports. Connectors were glued at the inlet and outlet of the primary channel and at the outlet of the reservoir channel.

The experimental setup consists of a single syringe pump (Fisher Scientific) and a viewing microscope (Leica 165FC) to observe the working of the device. Once the connectors were glued on, tubing was inserted into the connectors (PTFE microbore tubing, 0.032"ID x 0.056"OD, Cole-Parmer) in preparation for the experiment.

This process of fabrication is repeatable with consistent results each time. The master mold of SU-8 on silicon was kept constant and new devices were made by pouring and curing PDMS over it. Each process once the SU-8 mold is obtained takes about an hour.

3.2 Experiments with micro-beads

Devices developed at every stage described in the design process have been tested using the procedure described below.

The device was tested using polystyrene beads (PolySciences, Inc.). Polystyrene beads with a mean diameter $15\mu\text{m}$ were diluted in water. A concentration of the order of 10^5 beads per mL was used. This mixture was injected into the channel using the syringe pump through PDMS ports fixed at the inlet and outlet as seen in Figure 16 below. The experiment was conducted at concentrations of the order of 10^3 , 10^4 , 10^5 and 10^6 beads per mL and flow rates of 0.8, 1.0, 1.2, 1.4, 1.5, 1.75, 2.0, 3.0 mL/hr to obtain optimal trapping. Changing the flow rate altered the migration of the particle and the trapping location of the particle (w. r. t the spiral number).

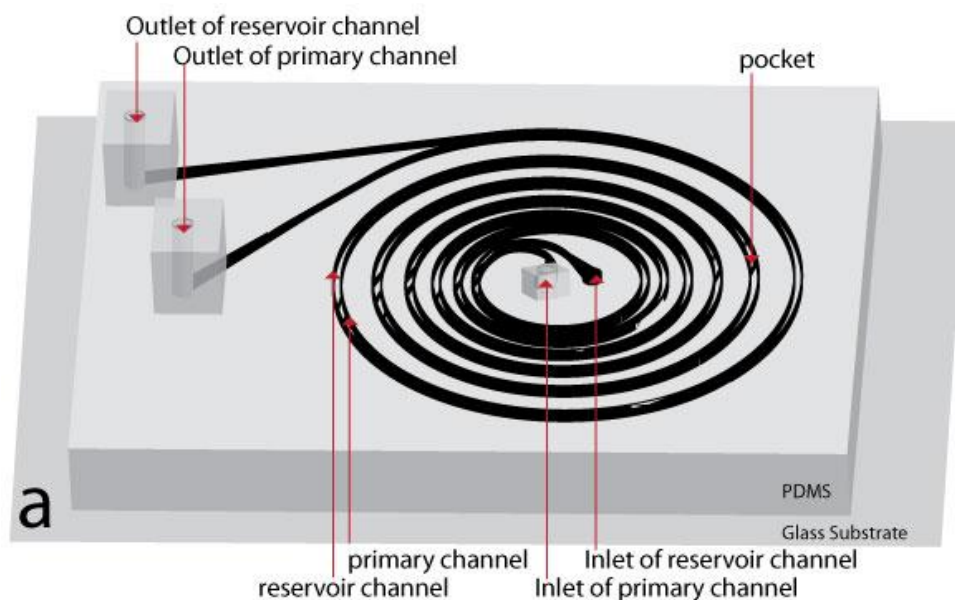


Figure 16: 3D view of the spiral device

It was clearly visible during the experiments that as the flow rate increased, the lateral migration of the particles occurred at shorter channel lengths and hence, at lower spirals. Hence flow rate also affected trapping. Particles moving very close to the outer wall were pushed into the pocket by the lateral fluid drag around the pocket region that was rushing into the pocket to equalize the pressure difference between the primary and secondary channel. Since the opening at the pocket is less than the diameter of the particle, the particle was fixated at the opening as show in Figure 16Figure 17. The cross-section of the opening of the outlet in each pocket is square, where as a bead circular. Since the trapped bead does not cover up the entire opening, there is dead space at the edges of the opening. This dead space provides suction and keeps the particle immobilized once it is trapped as seen in Figure 17 A.

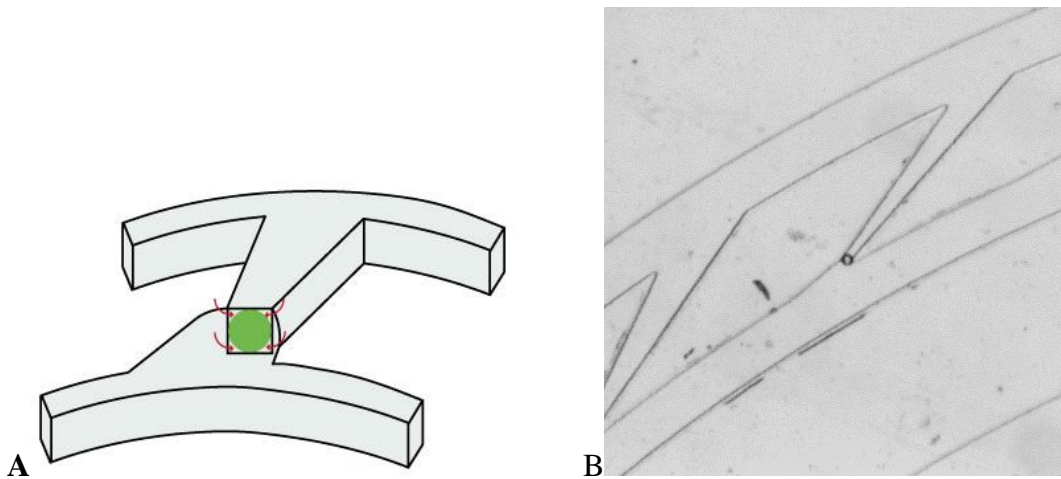


Figure 17: A) Depicts a trapped and immobilized particle B) Picture of a trapped and immobilized 30 μm glass bead.

A test was also conducted to observe the behavior of the device by using a particle with heavier mass and larger diameter. 30 μm glass beads (Polysciences Inc.) were used. The glass beads migrated towards the outer wall and once fixated in the pocket, did not escape.

No considerable change other than lateral migration distance was noticed when 30 μ m glass beads were used.

3.3 Experiments with animal cells

For cell trapping experiments, adult rat hippocampal stem cells were obtained (Sakaguchi Lab, Iowa State University). They express green fluorescent protein (GFP) and in suspension have a diameter of approximately 20 microns. Cells suspended in culture medium with a concentration of 3×10^5 cells/mL, were injected into the primary channel. Since the mass of each cell is less than the mass of a polystyrene bead, flow rates were adjusted accordingly.

Cells migrated towards the outer wall as seen in Figure 18 and it was possible to trap cells as seen in the Figure 20. These trapped cells were immobilized and this is a key advantage when you using this device for cell analysis. After the trapping phase of the experiment, in order to perform cellular analysis, cells can be treated with reagents through the reservoir channel.

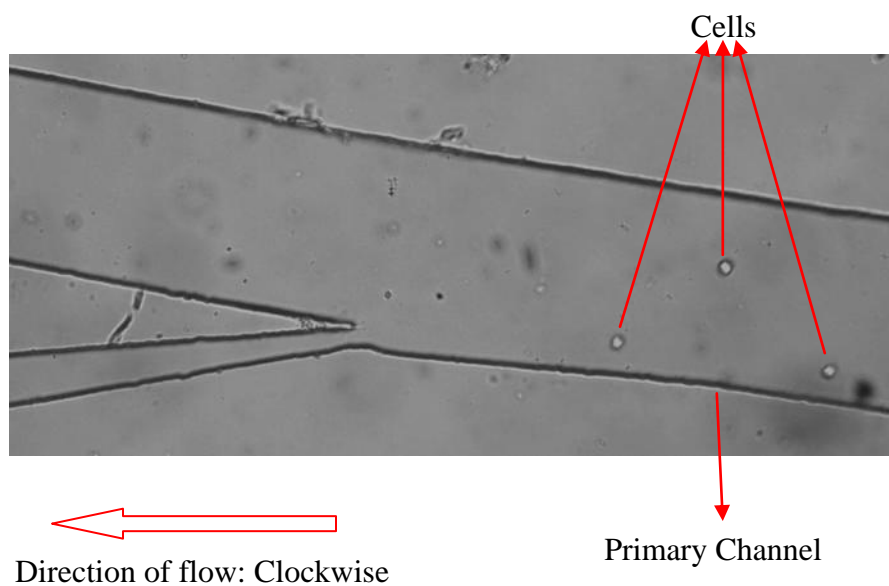


Figure 18: Picture showing cells that have migrated to the outer wall at Spiral 2 at a flow rate of 2.0mL/hr.

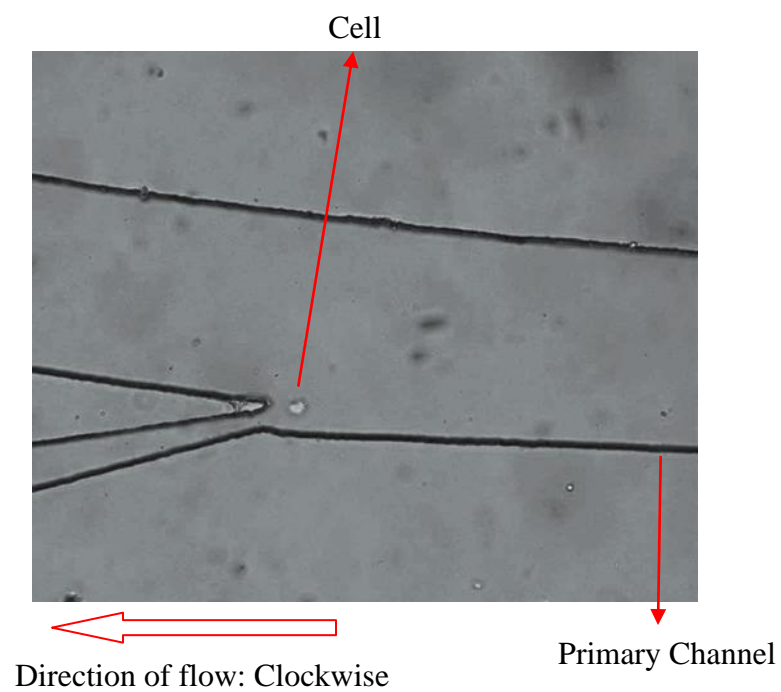


Figure 19: Picture of the cell migrating towards the pocket.

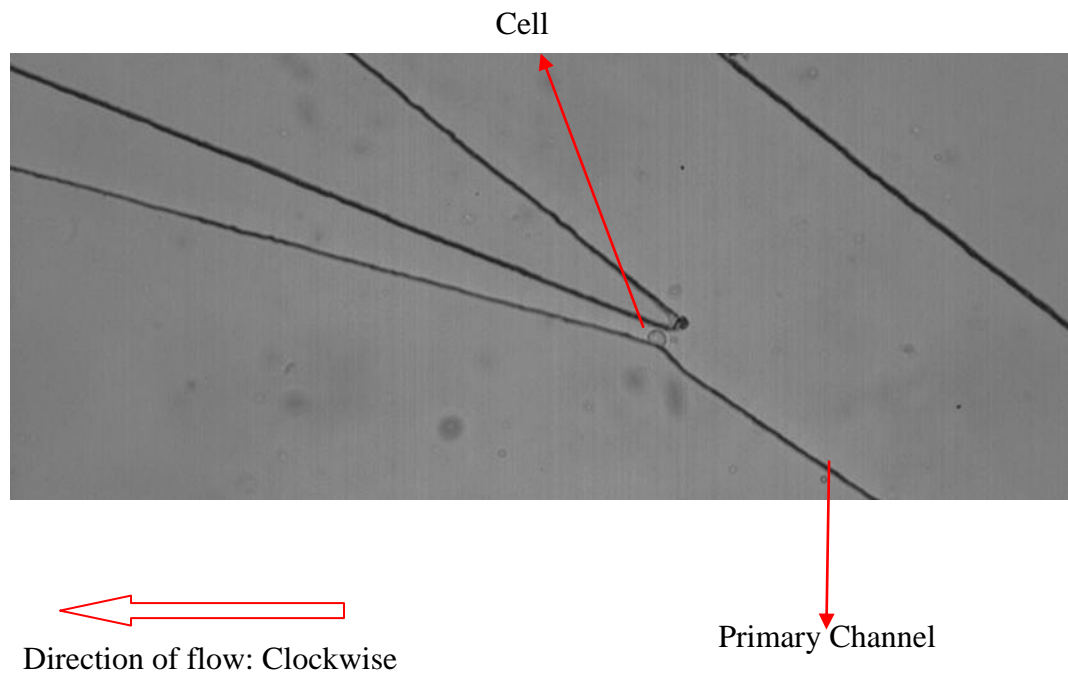


Figure 20: Picture of a cell trapped at the opening of the pocket

When the printed PDMS is exposed to air plasma to bond with glass, the surface chemistry gets affected as it changes from hydrophobic to hydrophilic (a temporary change). Though the PDMS surface eventually loses its hydrophilicity when it is left out for a long time, there may be some remnant hydrophilic regions in the channel. Cells get adsorbed to such small regions and are no longer buoyant in the fluid stream. This however, did not hinder the flow of other cells or trapping as seen through the microscope.

CHAPTER 4. RESULTS AND DISCUSSIONS

A complete understanding and proof of the device operation can be obtained on comparing the simulation results with the experimental results. As described previously, particles are injected into the primary channel. As they travel through regions of very high curvature, particles experience a high Dean Drag force since F_D is inversely proportional to the radius of curvature ($F_D \propto R^{-0.815}$) as seen in

$$F_D = f_L * \rho * U_f^2 * \frac{a^4}{D_H^2} = 5.4 * 10^{-4} * \pi \mu D e^{1.63} a_p (N) \quad \text{Equation 2}$$

Hence, in the initial spirals, the particles get entrained into one of the Dean vortices. As the particles travel through the channel, the radius of curvature keeps increasing and F_D decreases. The inertial lift forces begin to dominate and the particles get pushed out of the Dean vortices towards the outer wall of the channel since $F_D + F_L$ acting radially outward is higher in magnitude than $F_D - F_L$ acting radially inward. The particles reach their equilibrium positions and continue to traverse the channel until they get trapped.

Using the theoretical models, trapping of the particle can be predicted. The Dean number is calculated using Equation 1 (page 13) for each curvature. From the Dean number, the drag force F_D and the inertial lift force F_L that a particle experiences at each curvature change can be calculated using Equation 5 and Equation 6 respectively.

$$F_D = 5.4 * 10^{-4} * \pi \mu D e^{1.63} * a_p (N) \quad \text{Equation 5}$$

$$F_L = \rho * G^2 * C_L * a_p^4 \quad \text{Equation 6}$$

where G is the shear rate of the fluid (s^{-1}) and C_L is the lift coefficient which is a function of the particle position across the channel cross-section assuming an average value of 0.5 (27).

The average value of G for a Poiseuille flow is given by $G = U_{\max}/D_h$, where, U_{\max} is the maximum fluid velocity (ms^{-1}) and can be approximated as $2 * U_f$. Table 1 below predicts where trapping will take place. The highlighted region corresponds to that area in the channel or the spiral number, where the inertial lift force (Table 2) is $F_L \geq$ Dean Drag force F_D , causing particles to migrate towards the outer wall and get trapped.

Table 1: Dean Drag force experienced by particles at each radius of curvature for different injection rates of 15 μ m polystyrene particles.

Spiral	Radius of Curvature R (m)	Fluid Velocity, U_f (mL/hr)						Dean Drag Force (N)
		0.8	1.2	1.4	1.8	2.0	3.0	
1	0.00606	2.89E-11	5.61E-11	7.21E-11	1.08E-10	1.28E-10	2.5E-10	
	0.015447	1.35E-11	2.62E-11	3.36E-11	5.06E-11	6.01E-11	1.16E-10	
2	0.017107	1.24E-11	2.41E-11	3.09E-11	4.66E-11	5.53E-11	1.07E-10	
	0.018583	1.16E-11	2.25E-11	2.89E-11	4.35E-11	5.17E-11	1E-10	
3	0.020605	1.06E-11	2.07E-11	2.66E-11	4.00E-11	4.75E-11	9.21E-11	
	0.023078	9.73E-12	1.89E-11	2.42E-11	3.65E-11	4.33E-11	8.4E-11	
4	0.025567	8.95E-12	1.73E-11	2.23E-11	3.36E-11	3.98E-11	7.72E-11	
	0.028084	8.29E-12	1.61E-11	2.07E-11	3.11E-11	3.69E-11	7.15E-11	
5	0.031309	7.59E-12	1.47E-11	1.89E-11	2.84E-11	3.38E-11	6.55E-11	
	0.034741	6.97E-12	1.35E-11	1.74E-11	2.61E-11	3.10E-11	6.02E-11	
	0.03813	6.46E-12	1.25E-11	1.61E-11	2.42E-11	2.87E-11	5.58E-11	

Table 2: Inertial Lift force experienced by particles at different fluid velocities

	Fluid Velocity, U_f (mL/hr)					
	0.8	1.2	1.4	1.8	2.0	3.0
Inertial Lift Force, F_L (N)	7.61E-12	1.71E-11	2.33E-11	3.85E-11	4.75E-11	1.07E-10

From the above table, it is clear that as the fluid velocity increases, particle migration and band focusing phenomenon begin to occur at earlier spirals (closer to the inlet). It is also interesting to see that by changing the radius of curvature, the Dean Drag force can be altered and there by the device can be designed to achieve band focusing at any desired spiral. These are key results that will be important for future applications of the device and other spiral microfluidic devices, in general.

4.1 Experiments with micro-beads

Before we present the final results of this project, it is important to see the results obtained at each design stage described in 2.3 Device design because these results have lead to the achievement of a final successful design.

4.1.1 Stage 1: Curvilinear channels with pockets

When particles suspended in water were pumped into the curvilinear channel device, migration of the particle to the outer wall was not noticed. As the speed was increased from 0.8mL/hr to 3ml/hr, no change was noticed.

At every curvature change, particles migrate slightly as the centrifugal force that they experience changes. During these experiments, since the migration was not visible, it was

ascertained that the particles had not travelled a sufficient length in the curved channel in order to experience a large enough centrifugal force to cause visible drift. Hence, no trapping was achieved as well, as seen in Figure 21.

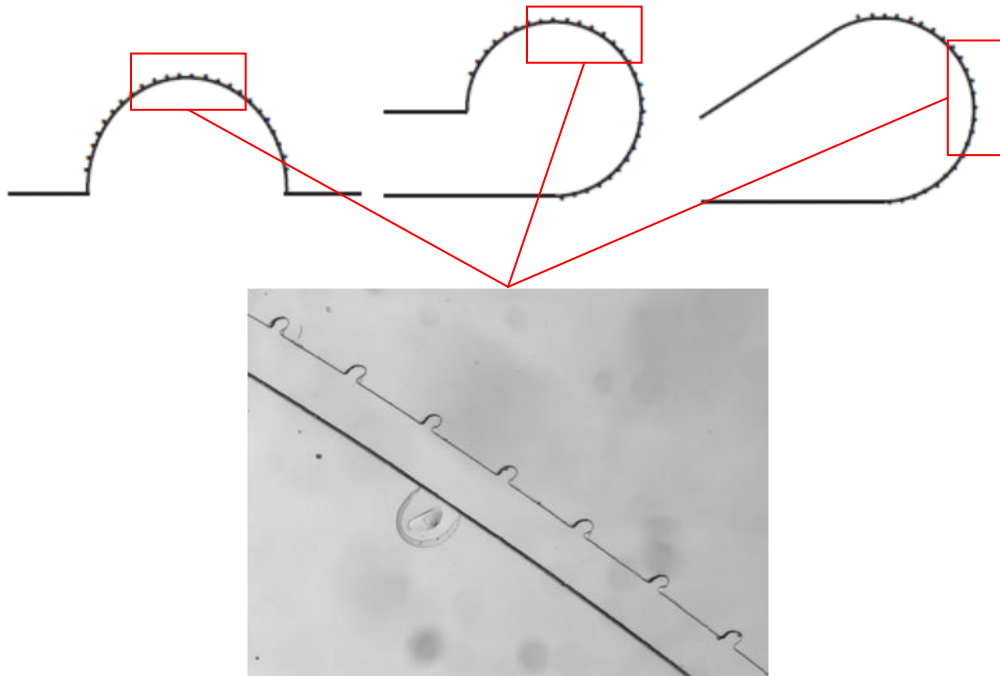


Figure 21: Curvilinear channel with pockets. No trapping obtained.

4.1.2 Stage 2: Spiral channel with pockets

An improvement made to the previous design was to extend the length of the channel by adding spirals. When the particle mixture was pumped into a different channels consisting of 4, 5 and 6 spirals respectively, lateral migration was clearly visible.

In accordance with the Table 1, changing the flow rate altered the migration of the particle and the trapping location of the particle (w. r. t the spiral number) during experiments. Figure 22 shows the visible migration of particles as they travel from the first

spiral (at the inlet) to the last spiral (at the outlet) at an injection rate at 1.2 mL/hr. Clearly visible in the pictures, is the migration of particles w.r.t to each successive spiral and finally accumulation of particles near the outer wall in the final spirals (4th and 5th).

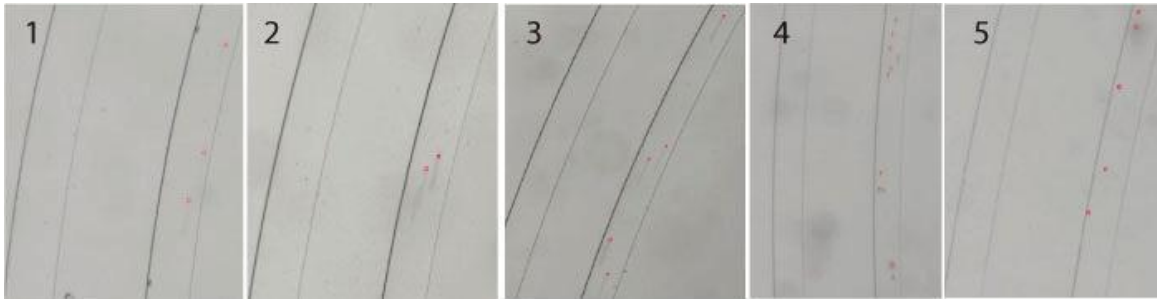


Figure 22: Demonstrates the migration of particles from inner wall towards the outer wall as they move from the first spiral (close to inlet) to the fifth spiral (close to outlet). These images belong to frames of a video recorded when a mixture of water and 15 μ m polystyrene beads was continuously injected into the channel at a speed of 1.2 mL/hr.

Although particle migration was successful, particle trapping still remained unattained.

4.1.3 Stage 3: Dual spiral channel with pockets

The working of this device matched exactly what was predicted during the design process. When particles migrated towards the outer wall, they began to flow close to the pockets. The pockets which have an opening leading to the reservoir channel have housed in them a local suction forced. When the fluid stream rushed in to equalize the pressure, particles flowing in that stream were carried along and got trapped at the opening inside the pocket. The particle remained fixated in this stable position.

In order to find an optimal flow rate for polystyrene beads and water mixture, it was injected into device at various flow rates. The concentration of beads in water was kept to $\sim 1 \times 10^5$ per mL for all trials. At low flow rates of 0.8 mL/hr, migration of particles was not noticeable under a microscope and particle trapping was not observed. When the flow rate was increased to 1.0 mL/hr, higher concentration of particle flow towards the outer wall was noticeable between the 4th and the 5th spiral.

Particles were trapped in all pockets from the 4th spiral to the last spiral. As seen in Figure 22, using a higher speed of 1.2 mL/hr, migration was noticed beginning in the 3rd spiral. As the particles reached the 3rd spiral, a sizeable number of them were seen flowing in the region between center of the channel and the outer wall. As seen in the table above, trapping occurs at the spirals ≥ 2 for flow rates of 3.0 mL/hr for 15 μ m polystyrene particles. Figure 24 illustrates trapping of beads at different locations in the spiral radially outward for spiral 2 to 5.

Figure 23 below is a snapshot image showing trails of passing polystyrene beads. These beads pass through an already filled pocket without getting trapped and thus maintaining single trapping – the objective of this experiment.



Figure 23: Still image from a video depicting polystyrene beads flowing past a filled pocket without entering the pocket. This demonstrates single trapping.

4.1.4 Stage 4: Increasing the number of traps in dual spirals

After achieving successful trapping, the only modification done at this stage was the addition of more pockets to increase the trapping efficiency. Increasing the number of traps did not affect trapping. Successful trapping was achieved in adjacent pockets ensuring the presence of a suction force at each pocket, even if they are not widely spaced, did not affect trapping, as seen in Figure 24 and Figure 25.

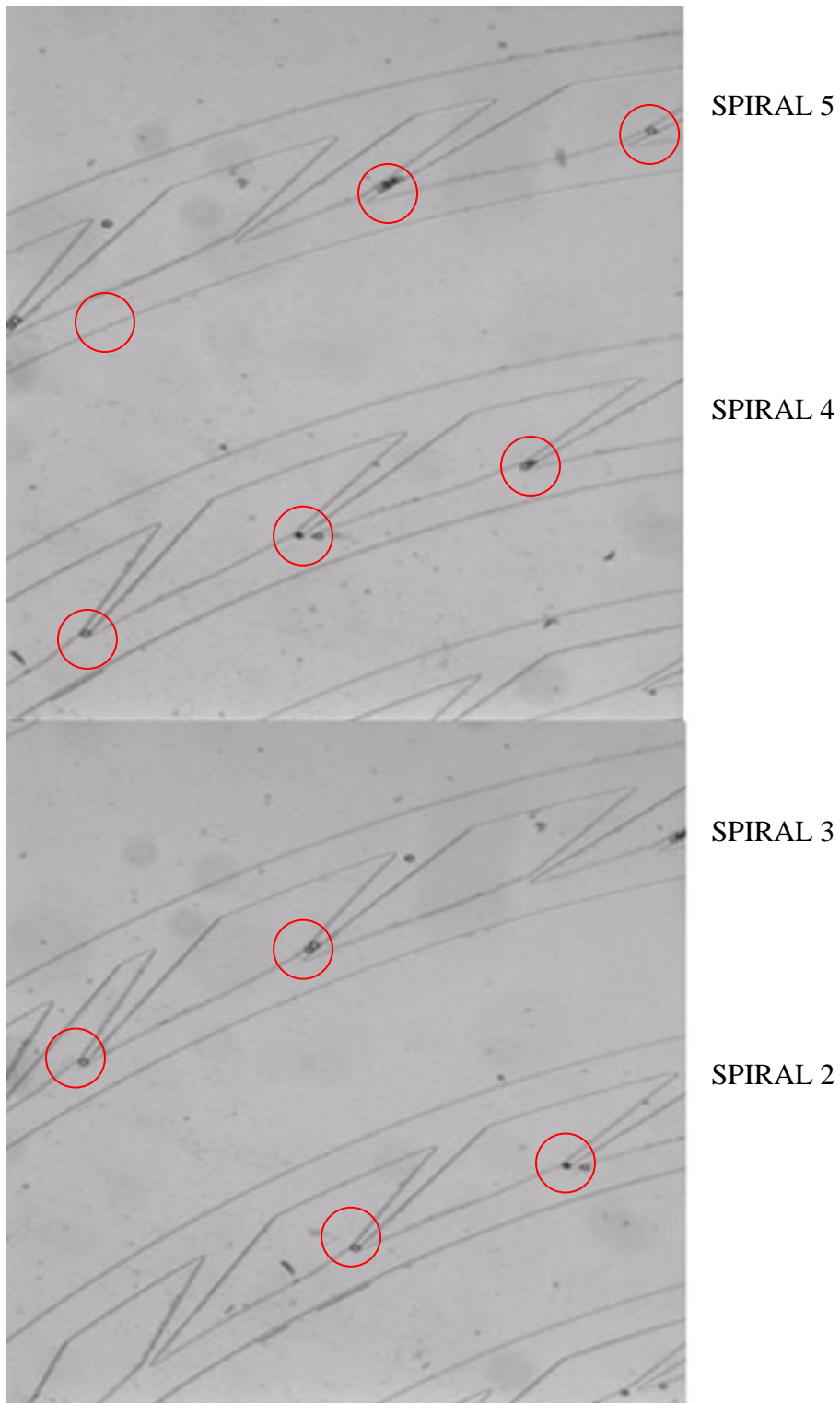


Figure 24: Collage containing picture snapshots taken radially outward for the 2nd spiral to the 5th spiral showing trapping in each spiral.

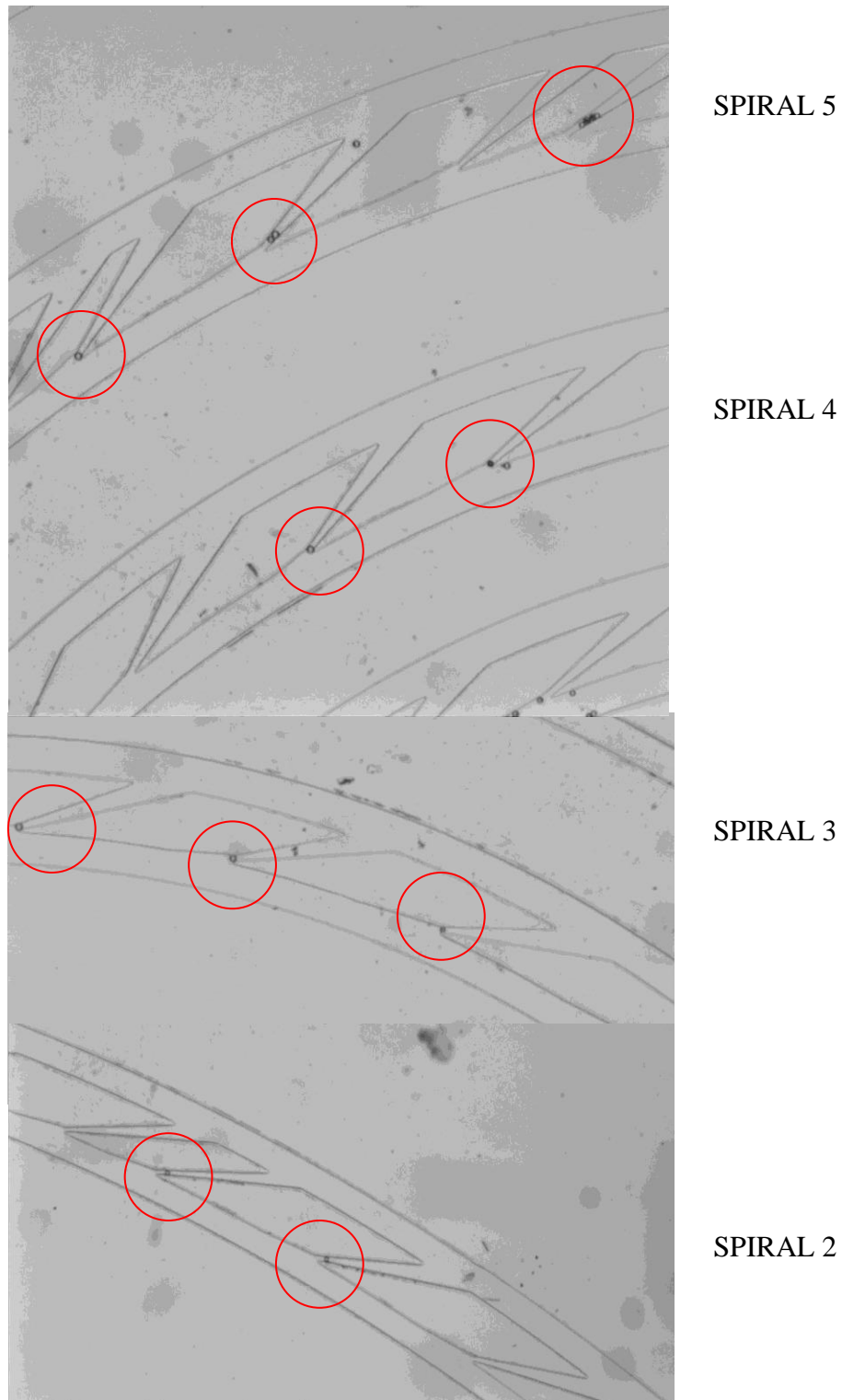


Figure 25: Collage containing picture snapshots taken radially outward for the 2nd spiral to the 5th spiral showing trapping in each spiral (different location in the spiral)

Trapping efficiency was calculated by flowing 30 μ m (size varied from 30-50 μ m) glass beads into the channel with height of <80 μ m in a spiral device with high density of pockets. As predicted in the simulations, the speed of the beads decreased as they travelled towards the outer spirals and fewer sites were trapped. Beads were injected in at 3.0 mL/hr and after a period of 10min, the trapping efficiency was calculated by counting the number of filled pockets. As seen in Table 3, trapping efficiency is the highest at the 3rd and the 4th spiral. Looking at Table 1 gives us an estimate of particle migration and trapping probability for an injection speed of 3.0 mL/hr. It is shown in the table, that trapping will occur after the 2nd spiral. This matches with the trapping efficiency values measured showing very high trapping at the 3rd and 4th spirals.

Table 3: Trapping Efficiency of pockets at each spiral

Spiral	No. of filled pockets	Total no. of pockets	% Trapping Efficiency
1	17	33	51.50
2	19	41	46.34
3	25	47	53.19
4	43	60	71.67
5	16	65	24.46

Trapping of cells at such low flow rates, in the order of a few mL/hr, cannot be obtained without a reservoir channel. It is only in conjunction with the reservoir channel, that

single trapping is obtained. This was proved by fabricating a device from Stage 1 of the design process Figure 21. Water and beads mixture was injected into the spiral channel with pockets but no reservoir. Particles migrated towards the outer wall, but did enter the pocket.

Increasing the flow rate beyond 2.0 mL/hr in 25 μ m high channels caused 2 distinct behaviors. Firstly, it created crowding of particles in the pockets located at the initial spiral (1st) depicted in Figure 26. A plausible explanation for this occurrence is illustrated in Figure 17A. The cross-section of the opening of the outlet in each pocket is square, where as a bead circular. Since the trapped bead does not cover up the entire opening, there is dead space at the edges of the opening. This dead space provides suction and can cause multiple trapping at higher flow rates. Another reason is that the centrifugal force is the largest at the smaller radius. Also, at high concentrations, the number of particles flowing close to the outer wall is dense and these can also cause over-crowding or multi-trapping. Secondly, when flow rates of 3 mL/hr and higher was used to inject the polystyrene bead mixture into the channel, leakage was noticed at the inlet. This can be avoided by increasing the height of the channel.

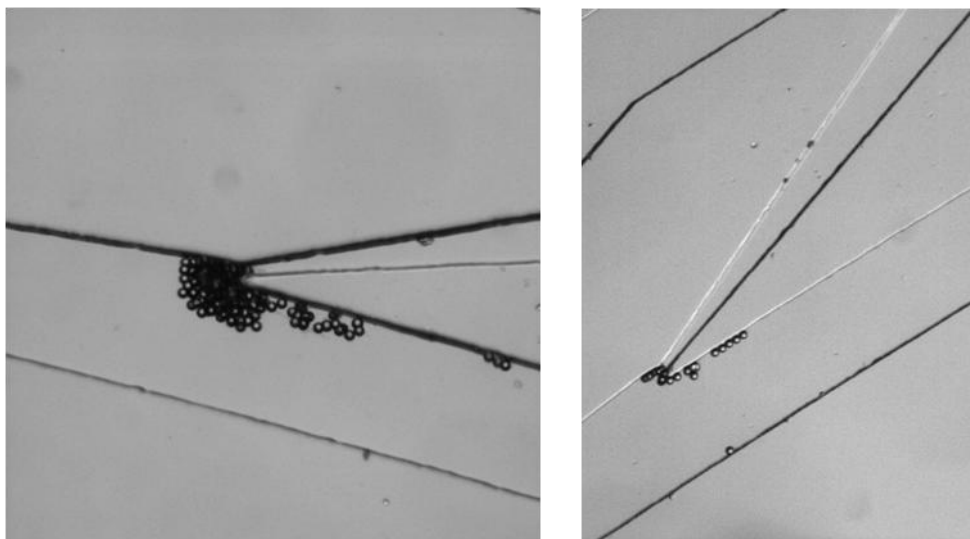


Figure 26: Crowding or accumulation of beads at pockets located in the first and second spiral noticed only when the flow rate is high (above 2.0 mL/hr)

4.2 Experiments with animal cells

The testing of the device using adult rat hippocampal stem cells was performed starting at a base flow rate of 1.2 ml/hr. The concentration of cells in the culture media was 1×10^5 cells per mL. Single cell trapping was obtained after the 5th spiral onwards and no cell crowding or accumulation was noticed in pockets at this flow rate. The device was tested with higher flow rates of 2.0 mL/hr and no cell accumulation was seen in the first two spirals as seen in Figure 27. Since the force acting on the media and cells is directly proportional to the mass the cells, the cells being lower in mass experience, experience a lower magnitude of lift and centrifugal forces. Hence, flowing polystyrene beads at 2.0 mL/hr caused crowding in pockets where as no crowding was seen when the experiment was performed with the cell mixture.

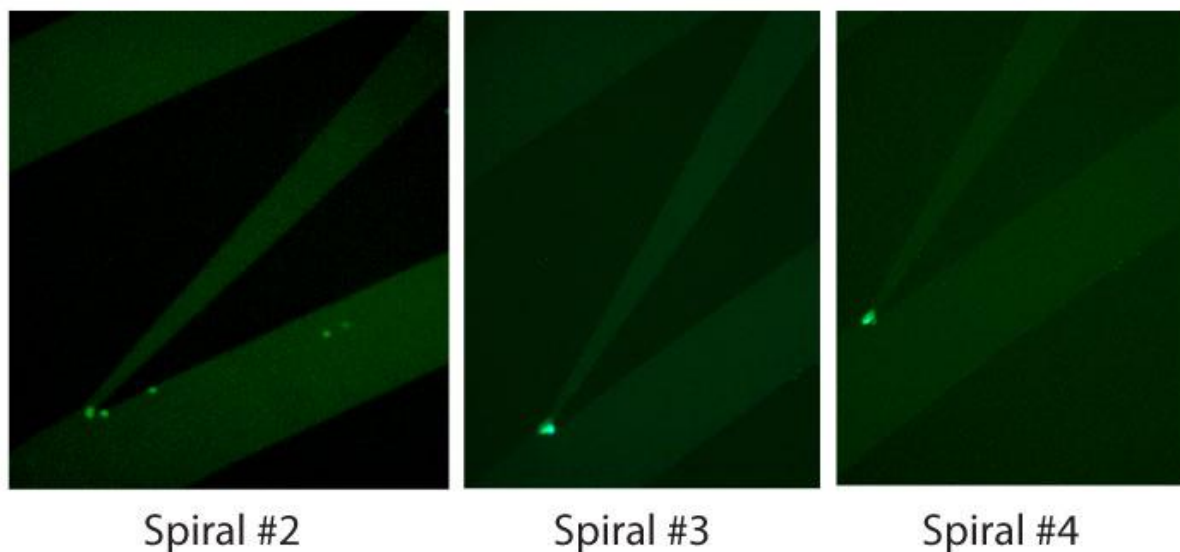


Figure 27: Single cell trapping using adult rat hippocampal stem cells when injected at the rate of 2.0 mL/hr. The concentration of the mixture used was 10^5 cells/mL.

Also, the cells near the outlet have experienced the greatest transverse shift and the probability of trapping is highest at this location due to the large concentration of cells near the outer wall and trapping occurs without pocket crowding.

Calibration of the device based on the size and mass of the cells is vital. This will allow single cell trapping starting at spirals closer to inlet, providing a larger distribution of data during cell analysis experiments. Table 4 below summarizes the performance of the device at different flow rates for both beads and cells.

Table 4: Trapping site occupancy based on flow rate.

Size	Flow Rate	Trapping Site
Polystyrene beads – mean diameter of 15μm	0.8 mL/hr	No trapping observed
	1.0 mL/hr	Spiral \geq 4
	1.2 mL/hr	Spiral \geq 3
Cells – mean diameter of 20 μm	0.8 mL/hr	No trapping observed
	1.0 mL/hr	Only in 2 pockets of Spiral 6
	1.2 mL/hr	Spiral \geq 5
	2.0 mL/hr	Spiral \geq 2

Hence, it is clear from above table that two things determine cell trapping – 1) Flow rate and 2) channel length travelled – spiral number.

CHAPTER 5. CONCLUSION AND FUTURE WORK

It has been demonstrated that spiral microfluidic channels can be used to separate target cells from a heterogeneous mixture. Combining fresh perspective on single cell trapping with a spiral device to achieve cell sorting and trapping is the gist of this thesis work. Trapping cells using centrifugal force has been tried before by one research group but with a major disadvantage that their device required a lot of additional electronics and centrifugation was generated externally (20).

It has been proven with simulation and experimental work, that this proposed design can be used to sort cells and trap cells. This was achieved using two 5 spiral channels – the primary channel for the injection of cells and trapping, and the reservoir channel to facilitate trapping, the collection excess media and cell analysis. With the use of pockets or traps at the outer wall of the primary channel, single cells can be collected. The pockets are 1.5 times the size of the target cell and hence only single trapping is achieved. It also allows for a larger variety of cells to be trapped. The reservoir channel, apart from being the back-bone of the device, brings forth many applications and cell studies that can be performed on this device. Using the reservoir channel, cells can be treated in a limited manner with environmental cues and chemical reagents. By controlling the amount of fluid through the reservoir channel, entire the cell can be exposed to the reagent, or by flowing reagent at a very low flow rate, it can be ensured that only a part of the fixated cell is exposed.

It must also be noted that single cell trapping using spiral microfluidic channels was obtained without the use of expensive equipment and fabrication procedures. A trapping

efficiency of higher than 50% was obtained in each spiral at relatively low flow rate of 3.0 mL/hr. There was good agreement between simulation predictions and experimental results.

Single cell trapping devices have a variety of applications in cell analysis and study. This dual spiral device has the potential to be used in a variety of applications. Studies have been conducted previously on single cells to test a variety of cellular behaviors and mechanisms as shown in Table 5.

This device has the potential to offer increasing concentration gradient generation, switch between buffer and reagent streams at each cell position using then primary and secondary channels respectively, and provide soluble cues and deliver chemicals in a controlled gradient using the long spiraling primary and secondary channels. A very uniform gradient can be created across the length of these long spirals. It can be tested for adhesion based cell separation and trapping. Hence there are a lot of avenues for future work related to the applications of this dual spiral microfluidic device.

Table 5: Summary of single cells analysis, properties of interest and method of analysis

Type of Cell	Property of Interest	Method
HL-60 Cells (31)	Monitor ATP-dependent calcium uptake	Trap and subject to analyte solution with a linearly increasing concentration gradient
Jurkat Cells (ionomycin-stimulated) (32)	Monitor very fast cellular responses	Very rapid fluidic switching between buffer and reagent stream at cell position
α-CD3-stimulated Jurkat cells (33)	mitogen-activated protein kinase responses	Soluble cues applied for varying time periods by mixing reagents in successive fluid compartments
Human neutrophils (34)	Test directional migration in simple and complex interleukin-8 (IL-8) gradients	Cells positioned in microchannel migrate towards increasing concentrations of IL-8 in linear gradients
HL60 promyelocytic leukemia cells expressing a transfected CXCR2 chemokine receptor (35)	Chemotaxis, the effects of flow on cell migration during chemotaxis	Chemicals delivered in a controlled gradient
White blood cells (36)	arrest fast-moving white cells that bear complementary ligands to specialized proteins including the selectin family	Adhesion based cell collection and separation
HL-60 and U-937 (37)	Using E-selectinIgG chimera coated on channel walls	Adhesion based cell collection and separation
T-lymphocytes (38)	specificity of this antibody to the CD5 surface antigen	Adhesion based cell collection and separation

BIBLIOGRAPHY

1. *Diffusion dependent cell behavior in microenvironments.* **Hongmei Yu, Ivar Meyvantsson, Irina A. Shkelab and David J. Beebe.** 1089–1095, s.l. : Lab on Chip, RSC, 2005, Vol. 5.
2. *The mechanical properties of Saccharomyces cerevisiae.* **Smith, A. E., Z. Zhang, C. R. Thomas, K. E. Moxham, and A. P. J. Middelberg,** 9871-9874, s.l. : Proc. Natl. Acad. Sci, 2000, Vol. 97.
3. *Atomic force microscopy and theoretical considerations of surface properties and turgor pressures of bacteria.* **Yao, X., J. Walter, S. Burke, S. Stewart, M. H. Jericho, D. Pink, R. Hunter, and T. J. Beveridge.** 213-230, s.l. : Colloids Surf. Ser. B, 2002, Vol. 23.
4. *The origins and the future of microfluidics.* **Whitesides, George M.** 368-373, s.l. : Nature , 2006, Vol. 442.
5. *Microfluidics: a new cosset for neurobiology.* **Jinyi Wang, Li Ren, Li Li, Wenming Liu, Jing Zhou, Wenhao Yu, Denwen Tong and Shulin Chen.** 644-652, s.l. : Lab on a Chip, 2009, Vol. 9.
6. *A centrifugation-enhanced high efficiency micro filter with spiral channel.* **Xu Ji, Wei Wang, Xia Lou, Jianhong Peng, and Zhihong Li.** Lyon, France : Transducers and EuroSensors, 2007.
7. *Continuous particle separation in spiral microchannels using dean flows and.* **Ali Asgar S. Bhagat, Sathyakumar S. Kuntaegowdanahalli and Ian Papautsky.** 1906-1914, s.l. : Lab on Chip, RSC, 2008, Vol. 8.

8. *Self-sorting of white blood cells in a lattice.* **R. Carlson, C. Gabel, S. Chan, R. Austin.** 2149–2152, s.l. : Physical Review Letters, 1997, Vol. 79.
9. *Filter-based microfluidic device as a platform for immunofluorescent assay of microbial cells.* **L. Zhu, Q. Zhang, H.H. Feng, S. Ang, F.S. Chau, W.T. Liu.** 337, s.l. : Lab on Chip, 2004, Vol. 4.
10. *Molded polyethylene glycol microstructures for capturing cells within microfluidic channels.* **A. Khademhosseini, J. Yeh, S. Jon, G. Eng, K.Y. Suh, J.A. Burdick, R. Langer.** 425-300, s.l. : Lab on a Chip, 2004, Vol. 4.
11. *Electrothermally activated SU-8 microgripper for single cell manipulation in solution.* **N Chronis, LP Lee.** 857, s.l. : Journal of Microelectromechanical Systems, 2005, Vol. 14.
12. *Sizing, Fractionation and Mixing of Biological Objects via Microfabricated Devices.* **O. Bakajin, R. Carlons, C. Chou, S. Chan, C. Gabel, J. Knight.** s.l. : microTAS, 1998.
13. *Direct integration of micromachined pipettes in a flow channel for single DNA molecule study by optical tweezers.* **C. Rusu, R. van't Oever, M. de Boer, H. Jansen, J. Berenschot, J. Bennink, J. Kanger, B. de Grooth, M. Elwenspoek, J. Grever, J. Brugger, A. van den Berg.** 238–247, s.l. : Journal of Microelectromechanical Systems, 2001, Vol. 10.
14. *High-speed separation system of randomly suspended single living cells by laser trap and dielectrophoresis.* **F. Arai, A. Ichikawa, M. Ogawa, T. Fukuda, K. Horio, K. Itoigawa.** 283, s.l. : Electrophoresis, 2001, Vol. 22.

15. *On-chip single-cell microcultivation assay for monitoring environmental effects on isolated cells.* **S. Umehara, Y. Wakamoto, I. Inoue, K. Yasuda.** 3, s.l. : Biochemical and Biophysical Research Communications, 2003, Vol. 305.
16. *High-speed separation system of randomly suspended single living cells by laser trap and dielectrophoresis.* **Arai F, Ichikawa A, Ogawa M, Fukuda T, Horio K, Itoigawa K.** 283-288, s.l. : Electrophoresis, 2001, Vol. 22.
17. *Blood-on-Chip.* **M. Toner, D. Irimia, Annu.** 77, s.l. : Annual Review of Biomedical Engineering, 2005, Vol. 7.
18. *Manipulation of biological cells using a microelectromagnet matrix.* **H. Lee, A.M. Purdon, R.M. Westervelt.** 1063, s.l. : Applied Physics Letters, 2004, Vol. 85.
19. *Membrane-free microfiltration by asymmetric inertial migration.* **Jeonggi Seo, Meng H. Lean, Ashutosh Kole.** s.l. : Applied Physics Letters, 2007, Vol. 91.
20. *Single cell assay on CD-like lab chip using centrifugal single cell trap.* **Sung-Woo Lee*, **, In-Hye Lee, Sung-Shin Ryu, Seung-Min Kwak, Kyeong-Sik Shin, Ji-Yoon Kang, Hyo-Il Jung, Tae-Song Kim.** Kobe, Japan : MEMS, 2007.
21. *Inertial microfluidics.* **Carlo, Dino Di.** 3038–3046, s.l. : Lab on Chip, RSC, 2009, Vol. 9.
22. *Flow in curved pipes.* **S. A. Berger, L. Talbot and L. S. Yao.** 461–512, s.l. : Annu. Rev. Fluid Mech., 1983, Vol. 15.
23. *Inertial Migration of a Sphere in Poiseuille Flow.* **Hinch, J. A. Schonberg and E. J.** 517–524, s.l. : Journal of Fluid Mechanics, 1989, Vol. 203.
24. *Inertial Migration of Rigid Spherical Particles in Poiseuille Flow.* **J. Matas, J. F. Morris and E. Guazzelli.** 171–195, s.l. : Journal of Fluid Mechanics, 2004, Vol. 515.

25. *Experiments on the lift and drag of spheres suspended in a Poiseuille flow.* **Small, R. Eichhorn and S.** s.l. : Journal of Fluid Mechanics, 2006.

26. *Continuous inertial focusing, ordering, and separation of particles in microchannels.* **D. Di Carlo, D. Irimia, R. G. Tompkins and M. Toner.** s.l. : Proc. Natl. Acad. Sci, 2007. 104, 18892–7.

27. *Particle Segregation and Dynamics in Confined Flows.* **D. Di Carlo, J. F. Edd, K. J. Humphry, H. A. Stone and M. Toner.** 094503–4, s.l. : Physical Review Letters, 2009, Vol. 102.

28. *Particle focusing mechanisms in curving confined flows.* **Carlo, D. R. Gossett and D. Di.** s.l. : Anal. Chem., 2009.

29. *Soft Lithography.* **Whitesides, Younan Xia and George M.** 153–84, s.l. : Annu. Rev. Mater. Sci, 1998, Vol. 28.

30. *Ultra rapid prototyping of microfluidic systems using liquid phase photopolymerization.* **C. Khoury, G. A. Mensing, and D. J. Beebe.** 50-55, s.l. : Lab on Chip, RSC, 2002, Vol. 2.

31. *Cell docking and on-chip monitoring of cellular reactions with a controlled concentration gradient on a microfluidic device.* **Yang, M. S., Li, C. W. & Yang, J.** 3991–4001, s.l. : Analytical Chem., 2002, Vol. 74.

32. *Microfluidic device for single-cell analysis.* **Wheeler, A. R.** 3581–3586, s.l. : Anal. Chem., 2003, Vol. 75.

33. *Cell stimulus and lysis in a microfluidic device with segmented gas-liquid flow.* **J. El-Ali, S. Gaudet, A. Gunther, P. K. Sorger & K. F. Jensen.** 3629–3636, s.l. : Anal. Chem, 2005, Vol. 77.

34. *A microfluidic system for controlling reaction networks in time.* **H. Song, J. D. Tice & R. F. Ismagilov.** 768–772, s.l. : Angew, Chem. Int. Edn Engl., 2003, Vol. 42.
35. *Neutrophil chemotaxis in linear and complex gradients of interleukin-8 formed in a microfabricated device.* **Noo Li Jeon, Harihara Baskaran, Stephan K. W. Dertinger, George M. Whitesides, Livingston Van De Water & Mehmet Toner.** 826–830, s.l. : Nature Biotechnology, 2002, Vol. 20.
36. *Effects of flow and diffusion on chemotaxis studies in a microfabricated gradient generator.* **G. M. Walker, J. Sai, A. Richmond, M. Stremmer, C.Y. Chung, J.P. Wikswo.** 611–618, s.l. : Lab Chip, 2005, Vol. 5.
37. *Biomimetic technique for adhesion-based collection and separation of cells in a microfluidic channel.* **W. C. Chang, L. P. Lee, and D. Liepmann.** 64–73, s.l. : Lab Chip, 2005, Vol. 5.
38. *Development of a microfabricated cytometry platform for characterization and sorting of individual leukocytes.* **A. Revzin, K. Sekine, A. Sin, R. G. Tompkins and M. Toner.** 30-37, s.l. : Lab Chip , 2005, Vol. 5.

ACKNOWLEDGEMENTS

I would like to take this opportunity to thank many people who have guided and helped me in conducting this research. Thank you to Prof. Liang Dong for being my graduate advisor, guiding me through this project and funding my research. I would like to thank Thomas Schultz, Department of Agronomy for funding my degree. It would have been impossible to complete this masters degree without their constant financial support. I would like to thank Dr. Don Sakaguchi and Jisun Oh for providing us with animal cells to complete the testing of the device. Thank you to Dr. Jaeyoun Kim and Dr. Nathan Neihart for serving on my committee. I would like to thank Jiwon Lee for her constant support and friendship through this period. Lastly, I would like to thank all my friends and labmates for making these years very memorable with their friendship and presence. Last but not least, a big thank you to my family for believing in me and being my greatest moral support.